Biogeosciences Discuss., 11, 16391–16445, 2014
www.biogeosciences-discuss.net/11/16391/2014/
doi:10.5194/bgd-11-16391-2014

Biogeosciences
Discussions
Open Access

Spatial variability and temporal dynamics of greenhouse gas (CO_2, CH_4, N_2O) concentrations and fluxes along the Zambezi River mainstem and major tributaries

C. R. Teodoru[1], F. C. Nyoni[2], A. V. Borges[3], F. Darchambeau[3], I. Nyambe[2], and S. Bouillon[1]

[1]KU Leuven, Department of Earth and Environmental Sciences, Leuven, Belgium
[2]University of Zambia, Integrated Water Research Management Center, Lusaka, Zambia
[3]University of Liège, Chemical Oceanography Unit, Liège, Belgium

Received: 22 October 2014 – Accepted: 1 November 2014 – Published: 27 November 2014

Correspondence to: C. R. Teodoru (teo.teodoru@ees.kuleuven.be)

Published by Copernicus Publications on behalf of the European Geosciences Union.

Abstract

Spanning over 3000 km in length and with a catchment of approximately 1.4 million km^2, the Zambezi River is the fourth largest river in Africa and the largest flowing into the Indian Ocean from the African continent. As part of a broader study on the riverine biogeochemistry in the Zambezi River basin, we present data on greenhouse gas (GHG, carbon dioxide (CO_2), methane (CH_4), and nitrous oxide (N_2O)) concentrations and fluxes collected along the Zambezi River, reservoirs and several of its tributaries during 2012 and 2013 and over two climatic seasons (dry and wet) to constrain the interannual variability, seasonality and spatial heterogeneity along the aquatic continuum. All GHGs concentrations showed high spatial variability (coefficient of variation: 1.01 for CO_2, 2.65 for CH_4 and 0.21 for N_2O). Overall, there was no unidirectional pattern along the river stretch (i.e. decrease or increase towards the ocean), as the spatial heterogeneity of GHGs appeared to be determined mainly by the connectivity with floodplains and wetlands, and the presence of man-made structures (reservoirs) and natural barriers (waterfalls, rapids). Highest CO_2 and CH_4 concentrations in the mainstream river were found downstream of extensive floodplains/wetlands. Undersaturated CO_2 conditions, in contrast, were characteristic for the surface waters of the two large reservoirs along the Zambezi mainstem. N_2O concentrations showed the opposite pattern, being lowest downstream of floodplains and highest in reservoirs. Among tributaries, highest concentrations of both CO_2 and CH_4 were measured in the Shire River whereas low values were characteristic for more turbid systems such as the Luangwa and Mazoe rivers. The interannual variability in the Zambezi River was relatively large for both CO_2 and CH_4, and significantly higher concentrations (up to two fold) were measured during wet seasons compared to the dry season. Interannual variability of N_2O was less pronounced but generally higher values were found during the dry season. Overall, both concentrations and fluxes of CO_2 and CH_4 were well below the median/average values reported for tropical rivers, streams and reservoirs. A first-order mass balance suggests that carbon (C) transport to the ocean represents

the major component (59 %) of the budget (largely in the form of DIC), while only 38 % of total C yield is annually emitted into the atmosphere, mostly as CO_2 (98 %), and 3 % is removed by sedimentation in reservoirs.

1 Introduction

Contrary to the earlier perception of inland waters as simple pipelines passively transporting significant amounts of both organic and inorganic carbon (C) to the ocean, it is increasingly recognized that freshwater ecosystems are capable of processing large quantities of C derived from the surrounding landscape, being therefore active components of global C cycling. Global figures based on recent data compilations suggest that the amount of C processed and emitted into the atmosphere from inland waters offsets the overall C transport to the global ocean (Cole at al., 2007; Tranvik et al., 2009; Aufdenkampe et al., 2011; Bastviken et al., 2011; Butman and Raymond, 2011; Raymond et al., 2013). This amount of terrestrial C processed in rivers, lakes, and reservoirs reaches approximately half the magnitude of the oceanic CO_2 sink (IPCC, 2013), a value that is similar or even higher in magnitude than C uptake by terrestrial ecosystem (Aufdenkampe et al., 2011; IPCC, 2013). Despite large uncertainties related to these global estimates, it is evident that freshwater ecosystems play a vital role in C budgets, disproportional to their areal extent (Cole at al., 2007). Quantifying the role of freshwater ecosystems as C sources and sinks, understanding the link between terrestrial and aquatic ecosystem as well as the underlying biogeochemical processes are therefore fundamental for quantitative estimates of the impact of land use-related changes in C dynamics and for improving estimates of ecosystem C budgets.

Although rivers represent key elements of freshwater ecosystems, their role in global or regional C budgets remains yet unclear. Resulting from inputs of dissolved inorganic C (DIC) groundwater and from the mineralization of terrestrial organic C (OC) (Battin et al., 2008), supersaturation in CO_2 has been reported for large rivers in boreal, temperate and tropical areas (Cole and Caraco, 2001; Raymond and Cole, 2001; Richey

BGD
11, 16391–16445, 2014

Spatial variability and temporal dynamics of GHG concentrations and fluxes along the Zambezi River

C. R. Teodoru et al.

et al., 2002; Bouillon et al., 2014; Abril et al., 2014a). Studies of CO_2 dynamics in low-order rivers in temperate and boreal regions have also shown that these systems are extremely dynamic in terms of DIC (Guasch et al., 1998; Worrall et al., 2005; Waldron et al., 2007), and generally highly supersaturated in CO_2 (Kling et al., 1991; Hope et al., 2001; Finlay, 2003; Teodoru et al., 2009). However, data on tropical rivers and streams are particularly scarce compared to other regions despite their high contribution (more than half) to the global freshwater discharge to the ocean, and particular high importance in terms of riverine transport of sediments and C (Ludwig et al., 1996; Schlünz and Schneider, 2000) and the suggested higher areal CO_2 outgassing rates than temperate or boreal rivers (Aufdenkampe et al., 2011). While our understanding of C dynamics in tropical regions comes mostly from studies of the Amazon River Basin, up to date only a handful of studies explored the biogeochemical functioning of equally important African rivers (Koné et al., 2009, 2010; Bouillon et al., 2009, 2012, 2014; Tamooh et al., 2012, 2013; Wang et al., 2013; Mann et al., 2014; Marwick et al., 2014). Constraining the overall importance of rivers in global C budgets requires therefore an improved understanding of C cycling in other tropical and subtropical regions and systems which are currently overlooked.

As part of a broader study on catchment-scale biogeochemistry of African Rivers, the present study examines the spatio-temporal dynamics of CO_2, CH_4 and N_2O concentrations and fluxes in the Zambezi River Basin based on three sampling campaigns extended over two climatic seasons (wet 2012, wet 2013 and dry 2013). The study quantifies the magnitude of CO_2 and CH_4 concentrations and fluxes, identifies the main sources and the controlling factors responsible for the observed patterns, and examines hotspots for GHG exchange with the atmosphere. Finally, we make a first attempt at a C mass balance for the Zambezi River over the study period linking emissions, sinks and transport components of the balance to other known elements of C budgets.

BGD
11, 16391–16445, 2014

2 Materials and methods

2.1 The Zambezi River – general characteristics

The Zambezi River is the fourth largest river in Africa in terms of discharge after the Congo, Nile and Niger, and the largest flowing into the Indian Ocean from the African continent. The river originates in northwest Zambia (11.370° S, 024.308° E, 1450 m a.s.l.), and flows south-east over 3000 km before it discharges into the Indian Ocean in Mozambique (Fig. 1). Based on distinct geomorphological characteristics, the Zambezi River is divided into three major segments: (i) the Upper Zambezi from the headwaters to the Victoria Falls, (ii) the Middle Zambezi, from the Victoria Falls to the edge of the Mozambique coastal plain (below Cahora Bassa Gorge), and (iii) the Lower Zambezi, the stretch traversing the coastal plain down to the Indian Ocean (Wellington, 1955; Moor et al., 2007). The upper reaches of the river are incised into Upper Precambrian crystalline basement rocks composed of metamorphosed sediments including shale, dolomite and quartzite. Further downstream, the Zambezi widens into the Barotse Floodplain, a very low gradient stretch that traverses unconsolidated sands, known as the Kalahari Sand (loose sands, gravel, clay and marls). Downstream of the Barotse Floodplains, the gradient of the Zambezi steepens and the river begins to incise into Karoo-age basalts and sediments (sandstone, shale, limestone) that form the sub Kalahari bedrock, creating a series of rapids (Katima, Mambova, Katombora) and falls with the Victoria Falls (world's second largest: 1708 m width, 108 m height) marking the edge of the Upper Zambezi stretch (Moor et al., 2007). The Middle Zambezi, is characterized by a markedly steeper gradient than the section above the falls with an initial turbulent course through a series of narrow zigzag gorges and rapids (i.e. Batoka Gorge, Chimamba Rapids) before the river widens into the broad basins of the Kariba and Cahora Bassa reservoirs. Karoo-age basalts and sediments and subordinate Precambrian crystalline basement rocks (gneiss and granite) constitute the bedrock over most of this stretch of the river (Moor et al., 2007). Downstream of the Cahora Bassa Reservoir, the river flows through one last gorge (the Cahora Bassa Gorge) before

BGD
11, 16391–16445, 2014

entering a more calm and broader stretch of the Lower Zambezi. Traversing the Cretaceous and Tertiary sedimentary cover of the Mozambique coastal plain, the lower reaches of the river forms a large, 100 km long floodplain-delta system of oxbows, swamps, and multichannel meanders.

Along its course, the Zambezi River collects water from many tributaries from both left and right banks (including Luena, Lungue Bungo, Kabompo, Luangina, Cuando-Chobe, Gwayi, Shangani, Kafue, Luangwa, Mazoe and Shire, Fig. 1) which contribute with different proportion to the annual average discharge, which range between 3424 and 4134 $m^3 s^{-1}$ (Beilfuss and dos Santos, 2001; World Bank, 2010). With a mean discharge of 320 $m^3 s^{-1}$, the Kafue River is the major tributary of the Zambezi. The river originates in northwest Zambia, flows south, south-east for over 1550 km and joins the Zambezi River ~ 70 km downstream of the Kariba Dam. Its drainage basin of over 156 000 km^2 which lies entirely within Zambia is home to almost half of the country's population, and has a large concentration of mining, industrial and agricultural activities.

There are two major impoundments along the Zambezi River. The Kariba Reservoir, completed in 1959 between Zambia and Zimbabwe about 170 km downstream of the Victoria Falls (Fig. 1), is the world's largest reservoir by volume (volume: 157 km^3; area: 5364 km^2, Kunz et al., 2011a). Completed in 1974 in Mozambique, about 300 km downstream of the Kariba Dam (Fig. 1), the Cahora Bassa Reservoir is the fourth largest reservoir in Africa (volume: 52 km^3; area: 2675 km^2, Beilfuss and dos Santos, 2001). Contemporaneous with the construction of the Cahora Bassa Dam, two smaller reservoirs have been created on the Kafue River: (i) the Kafue Gorge Reservoir (volume: ~ 1 km^3; area: 13 km^2) completed in 1972 about 75 km upstream from the confluence with the Zambezi with the purpose of power generation, and (ii) the Itezhi Tezhi Reservoir (volume: ~ 6 km^3, area: 365 km^2) completed in 1978 about 270 km upstream (Fig. 1), as storage reservoir to ensure constant water supply for the Kafue Gorge. Several smaller dams have also been constructed on other tributaries including the Lunsemfwa Dam on the Lunsemfwa River, the Mulungushi Dam on the Mulungushi

BGD
11, 16391–16445, 2014

River, the Nkula Falls, Tedzani and Kapichira dams on the Shire River (World Bank, 2010), making the Zambezi River the most dammed river in Africa. Given the still large hydropower potential of the basin (up to 13 000 megawatts (MW) of which only 40 % is presently used), more than 16 hydropower projects are currently planned or under construction (World Bank, 2010).

The climate of the Zambezi basin, classified as humid subtropical, is generally characterized by two main seasons: the rainy season from October/November to April/May, and the dry season from May/June to September/October (Fig. 2). Annual rainfall across the river basin (mean 940 mm for the entire catchment) varies with latitude from about 400 to 500 mm in the extreme south and southwest part of the basin to more than 1400 mm in the northern part and around Lake Malawi (Chenje, 2000). Up to 95 % of the annual rainfall in the basin occurs during the rainy season while irregular and sporadic rainfall events during the dry period contribute generally up to 5 %. Driven by seasonality in rainfall patterns, the hydrological cycle of the Zambezi River has a bimodal distribution, characterized by a single main peak flood with maximum discharge occurring typically in April/May and minimum in November. An example of the seasonality and the disturbance of the natural flow pattern associated with river damming is illustrated in Fig. 2, based on daily discharge data measured at the Victoria Falls power station and at the Kariba Dam (on the Zambezi River) and at the Hook Bridge (upstream of the Itezhi Tezhi Reservoir) and the Kafue Gorge Dam (on the Kafue River) between January 2012 and January 2014.

Almost 75 % of the land area in the basin is covered by forest and bush. Cropped land (with mostly rain-fed agriculture) covers up to 13 %, and grassland cover about 8 % of the land area (SADC et al., 2012). Over the last 20 yr, continuous deforestation in the Zambezi River Basin countries, mostly due to land clearance for agriculture and settlements, wood cut for charcoal production and wild bush fire, has led to substantial loss of forested land. Figures indicate that between 1990 and 2010, the area covered by forest in each basin country (not necessarily within the area of the Zambezi River Basin) has dropped 18 % in Zimbabwe, 10 % in Tanzania, 6 % in Malawi and Mozam-

BGD
11, 16391–16445, 2014

bique, 5 % in Botswana and Zambia, and 2 % in Angola and Namibia (SADC et al., 2012).

Wetlands, comprising swamps, marshes and seasonally inundated floodplains cover more than 5 % of the total basin area (SADC et al., 2012; McCartney et al., 2013). The most important wetlands in the basin are the Lungue Bungo Swamps, Luena Flats, Barotse Floodplain, Sesheke Maramba Floodplain, Lukanga Swamps, Kafue Flats and Luangwa Floodplain in Zambia, the Cuando-Linyanti-Chobe-Zambezi Swamps (including Eastern Caprivi and Chobe Swamps) in northeastern Namibia, the Mid-Zambezi Valley and Mano Pools in Zimbabwe, the Shire Marshes in Malawi and the Lower Zambezi and Zambezi Delta in Mozambique (McCartney et al., 2013).

In 1998, the population in the basin was estimated at 31.7 million (one-third of the total population of the eight basin countries), out of which more than 85 % lives in Malawi, Zambia and Zimbabwe. Ten years later (2008) the population reached over 40 million and it is predicted to achieve 51.2 million by 2025 (SADC et al., 2012). This predicted increase in population, alongside with ongoing economical development in the region and new hydropower projects is expected to exert further pressure on the aquatic environment and natural water resources of the basin.

2.2 Sampling strategy and analytical techniques

To account for interannual variability and seasonality, sampling was conducted during two consecutive years and over two climatic seasons: wet season (1 February to 5 May) 2012, wet season (6 January to 21 March) 2013, and dry season (15 October to 28 November) 2013 (Fig. 2). In addition, two sites, one on the Zambezi River (ZBZ.11 located ~ 5 km upstream of the confluence with Kafue) and on the Kafue River (KAF.10 located ~ 6 km upstream the confluence with Zambezi, Fig. 1) were monitored bi-weekly between 19 February 2012 and 22 November 2013 (data discussed in a companion paper). To address the spatial variability, up to 56 sites were visited each campaign, depending on logistics and accessibility. Sampling sites (chosen at 100–150 km apart) were located as follows: 26 along the Zambezi mainstream (includ-

BGD
11, 16391–16445, 2014

ing 3 sites on the Kariba and 3 on the Cahora Bassa reservoirs), 2 on the Kabompo, 13 along the Kafue (including 3 on the Itezhi Tezhi Reservoir), 3 on the Lunga (main tributary of the Kafue), 5 along the Luangwa, 2 on the Lunsemfwa (main tributary of the Luangwa), one on the Mazoe and one on the Shire River (Fig. 1). In situ measurements and water sampling was performed, whenever possible, from boats or dugout canoes in the middle of the river at ~ 0.5 m below the water surface. However, in the absence of boats/canoes, sampling was carried out either form bridges or directly from the shore and as much as possible away from the shoreline.

At each location, in situ measurements of water temperature, dissolved oxygen (DO), conductivity and pH were performed with a YSI ProPlus multimeter probe. The pH and DO probes were calibrated each time before the measurement using United States National Bureau of Standards buffer solutions of 4 and 7, and water saturated air. The partial pressure of CO_2 (pCO_2) in the water was measured in situ with a PP-Systems EGM-4 non-dispersive, infrared gas analyzer (calibrated before each field cruise with a certified gas standard with a mixing ratio of 1017 ppm) using both a Liqui-Cel Mini-iModule membrane contactor equilibrator and a headspace technique. For the first method, the water pumped from ~ 0.5 m depth, was circulated through the exchanger at a constant flow rate of ~ 0.35 L min^{-1}, and the gases were continuously re-circulated in a closed loop into the EGM-4 for instantaneous measurements of pCO_2. At a flow rate of 0.35 L min^{-1}, the half-equilibration time of CO_2 in the MiniModule is 4–5 s. For the headspace technique, 30 mL of water, collected (under the water) into five 60 mL polypropylene syringes was mixed with 30 mL air of known CO_2 concentration and gently shaken for 5 min allowing the equilibration of the two phases. The headspace volume (30 mL) was then transferred into a new syringe and directly injected into the EGM-4 analyzer. Water pCO_2 was calculated from the ratio between the air and water volumes using the gas solubility at sampling temperature. Comparison between the syringe-headspace and membrane equilibrator techniques gave consistent results with slope not significantly different from unity (1.09), $r^2 = 0.992$, $p < 0.0001$, $n = 83$, in the 140–14 000 ppm range (Abril et al., 2014b).

BGD
11, 16391–16445, 2014

CO_2 fluxes to the atmosphere were measured using a custom-designed floating chamber (Polyvinyl chloride cylinder of 38 cm internal diameter, 15 cm active height, plus 7 cm skirt under the air-water interface) connected at the top-most through 2 rubber-polymer tubes (Ø = 0.45 cm) to a non-dispersive infrared analyzer (PP-System, EGM-4). Starting at atmospheric concentration (and pressure), the air inside the chamber (17 L volume) was circulated in a closed loop and analyzed for CO_2 with readings every 1/2 min over a 30 min period. Temperature inside the chamber was monitored continuously with a VWR 4039 Waterproof Thermometer (accuracy ±1 °C) and further used in the flux calculation. For the determination of CH_4 fluxes, a 60 mL syringe, fitted on a third tube with a two-way valve was filled with 30 mL air from inside the chamber at 0, 5, 10, 20 and 30 min interval. Transferred immediately into a 50 mL septa vial, pre-filled with saturated saline solution, samples were stored in upside-down position until analyzed in the laboratory by gas chromatography (GC) (see below). Fluxes to atmosphere were estimated from the change in concentrations using the following equation:

$$F = \left[(s \cdot V)/(\text{mV} \cdot S)\right] \cdot f \tag{1}$$

where: F is the flux in µmol m^{-2} d^{-1}; s is the slope in µatm min^{-1}; V is the volume of the chamber in liters (L); mV (molar volume) is the volume of one mole of gas in L atm mol^{-1}; S is the surface area of the floating chamber over the water in m^2; and f is the conversion factor from minute to day (1 d = 1440 min) (see Teodoru et al., 2010). When possible, flux chamber measurements were performed on both static and drift-mode with constant records of water velocity (relative to the chamber for static mode) and drift velocity to account for the enhanced gas exchange coefficient due to local-induced turbulence by the chamber itself. At each location, before and after chamber measurements, additional ambient air $p\text{CO}_2$ concentration was measured by injecting air samples into the EGM-4 analyzer, while air temperature, barometric pressure, humidity and wind speed were measured at ~ 1 m above the water surface using a hand-held anemometer (Kestrel 4000, accuracy 3 %). Measurement precision

BGD
11, 16391–16445, 2014

of pCO_2 with the EGM-4 was ±1 %, and the stability/drift of the instrument (checked after each cruise), was always less than 2 %.

Samples for dissolved CH_4, N_2O and the stable isotope composition of dissolved inorganic C ($\delta^{13}C_{DIC}$) were collected in 50 mL serum bottles (for CH_4 and N_2O) and 12 mL exetainer vials (for $\delta^{13}C_{DIC}$) filled from the Niskin bottle (allowing water to overflow), poisoned with $HgCl_2$, and capped without headspace. Concentrations of CH_4 and N_2O were determined by the headspace equilibration technique (20 mL N_2 headspace in 50 mL serum bottles) and measured by GC (Weiss, 1981) with flame ionization detection (GC-FID) and electron capture detection (GC-ECD) with a SRI 8610C GC-FID-ECD calibrated with $CH_4 : CO_2 : N_2O : N_2$ mixtures (Air Liquide Belgium) of 1, 10 and 30 ppm CH_4 and of 0.2, 2.0 and 6.0 ppm N_2O, and using the solubility coefficients of Yamamoto et al. (1976) for CH_4 and Weiss and Price (1980) for N_2O. For the analysis of $\delta^{13}C_{DIC}$, a 2 mL helium (He) headspace was created, and H_3PO_4 was added to convert all DIC species to CO_2. After overnight equilibration, part of the headspace was injected into the He stream of an elemental analyser – isotope ratio mass spectrometer (EA-IRMS, ThermoFinnigan Flash HT and ThermoFinnigan DeltaV Advantage) for $\delta^{13}C$ measurements. The obtained $\delta^{13}C$ data were corrected for the isotopic equilibration between gaseous and dissolved CO_2 as described in Gillikin and Bouillon (2007), and measurements were calibrated with certified reference materials LSVEC and either NBS-19 or IAEA-CO-1.

For total alkalinity (TA), 80 mL of water samples were filtered on 0.2 µm polyethersulfone syringe filters (Sartorius, 16532-Q) and analysed by automated electro-titration on 50 mL samples with 0.1 $mol\,L^{-1}$ HCl as titrant (reproducibility was typically better than ±3 $\mu mol\,L^{-1}$ based on replicate analyses). DIC concentrations were computed from TA, pCO_2 and pH measurements using thermodynamic constants of Millero (1979) as implemented in the CO2SYS software (Lewis and Wallace, 1998). Using an estimated error for pH measurements of ±0.02 pH units, ±3 µM for TA, and ±0.1 °C for temperature, the propagated error for DIC is ±1 %. The concentrations of calcium (Ca), magnesium (Mg), and dissolved silica (DSi) were measured using inductively coupled plasma-

BGD
11, 16391–16445, 2014

atomic emission spectroscopy (Iris Advantage, Thermo Jarrel-Ash). The pelagic community respiration (R) rates were determined by quantifying the decrease in DO (with the optical DO probe YSI-ODO) using triplicate 60 mL Winkler bottles, incubated in a dark coolbox filled with water (to retain ambient temperature) for approximately 24 h. A respiratory molar oxidation ratio of 1.30 O_2 : C was used as the conversion rate from oxygen measurements into carbon (Richardson et al., 2013). The particulate primary production (P) rates in surface waters (i.e. not depth-integrated rates) were quantified in duplicate by determining the uptake of DIC after short-term (2–3 h) in situ incubations of river water during the day using 1 L polycarbonate bottles spiked with ^{13}C-labelled sodium bicarbonate ($NaH^{13}CO_3$). A subsample of the spiked water was sampled to measure the degree of ^{13}C-enrichment in the DIC pool. Samples for analysis of $\delta^{13}C_{POC}$ were obtained at the start (natural abundance values) and at the end of the incubation by filtering a known volume of surface water on pre-combusted (overnight at 450 °C) 25 mm GF/F filters (0.7 µm). Filters were decarbonated with HCl fumes for 4 h, re-dried and then packed into Ag cups. Particulate organic carbon (POC) and $\delta^{13}C_{POC}$ were determined on a Thermo elemental analyser – isotope ratio mass spectrometer (EA-IRMS) system (Flash HT with Delta V Advantage), using the thermal conductivity detector signal of the EA to quantify POC and by monitoring m/z 44, 45 and 46 on the IRMS. Quantification and calibration of δ^{13}C data were performed with IAEA-C6 and acetanilide that was calibrated against international standards. Reproducibility of $\delta^{13}C_{POC}$ measurements was typically better than 0.2 ‰. Calculations to quantify the rates were made as described in Dauchez et al. (1995). The R and P data here (in µmol C L^{-1} h^{-1}) refer only to surface water (~ 0.5 m deep) measurements and not to depth-integrated values.

BGD
11, 16391–16445, 2014

3 Results

3.1 Temporal and spatial variability of pCO_2

pCO_2 along the Zambezi River was highly variable, both spatially and temporally. Riverine pCO_2 was generally higher during wet seasons compared to the dry season (Fig. 3a). Lowest riverine values (i.e. excluding reservoirs) during wet seasons 2012 and 2013 of 640 and 660 ppm, respectively, were found immediately below the Victoria Falls, while highest concentrations were always recorded downstream of the Barotse Floodplains (7650 and 10 350 ppm, respectively) and downstream of the confluence with the Shire River in Mozambique (8180 and 12 200 ppm, respectively) (Fig. 3a). During the dry season of 2013, the lowest concentration (300 ppm, i.e. below atmospheric equilibrium) was measured at ZBZ.6 (~ 230 km upstream the Victoria Falls, Fig. 1), while highest pCO_2 was found at the river source and immediately below the Kariba Dam (2550 and 2600 ppm, respectively, Fig. 3a). Mean pCO_2 for the entire river (i.e. excluding reservoirs) was 2475 and 3730 ppm, respectively, during the wet season of 2012 and 2013, but only 1150 ppm (measurements up to ZBZ.13 only) during the dry season of 2013. Despite relatively large interannual variability (paired t test significantly different at 0.05 level, $p < 0.025$, $n = 15$), but low seasonality ($p < 0.09$, $n = 8$), pCO_2 along the Zambezi followed the same longitudinal pattern (slightly different during dry season) (Fig. 3a). The pCO_2 was always below atmospheric equilibrium in the surface water of the two major reservoirs (mean all campaigns 267 ppm for the Kariba and 219 ppm for the Cahora Bassa) with no distinct interanual variability or seasonality (Fig. 3a).

Large variability of riverine pCO_2 was also observed for the Kafue River (Fig. 3b). Excluding reservoir values, pCO_2 along the Kafue River varied between 905 and 1145 ppm during the wet season 2012 and 2013, respectively (both recorded at KAF. 6 located immediately below the Itezhi Tezhi Dam), up to 9985 and 11 745 ppm, respectively (both measured at KAF.8 in the Kafue Flats). Concentrations were consistently lower during the dry season 2013 ranging from 330 ppm at KAF.4 (below the Lukanga

BGD
11, 16391–16445, 2014

Swamps) up to 6650 ppm at the end of the Kafue Flats (KAF.9) (Fig. 3b). With a mean pCO_2 for the entire river of 3805 and 4748 ppm, respectively (without Ithezhi Tezhi Reservoir), concentrations in the Kafue were significantly different at 0.05 level during the two wet season campaigns (paired t test, $p < 0.009$, $n = 9$) as well as during 2013 dry season compared to 2013 wet season ($p < 0.026$, $n = 7$, mean 2770 ppm). pCO_2 in the surface water of the Itezhi Tezhi Reservoir was always above atmospheric concentration during both wet seasons (mean 1130 ppm in 2012 and 1554 ppm in 2013), showing a decreasing pattern with increasing the distance from the river inflow. The only measurement during dry season 2013 in the middle of the reservoir (ITT.2) indicated strong CO_2 undersaturated conditions (165 ppm). As observed for the Zambezi River, the variability of pCO_2 along the Kafue River followed a similar pattern during each campaign.

Overall, there was a good ($r^2 = 0.89$), negative correlation between pCO_2 and %DO for all sampled rivers, tributaries and reservoirs, and during all campaigns (Fig. 3c) with mostly reservoir samples characterized by DO oversaturation and low pCO_2, while DO undersaturation and high pCO_2 values (10 000–14 000 ppm) were characteristic for the Shire River, and several stations on the Zambezi and the Kafue Rivers, mostly downstream of floodplains. With an overall mean value of 2639 ppm over the entire sampled period, pCO_2 of the Zambezi River was 45 % lower than average pCO_2 of the Kafue River (mean 3852 ppm) (Fig. 4d). All other tributaries displayed also CO_2 supersaturated conditions with respect to atmospheric equilibrium with mean values ranging from as low as 955 and 1402 ppm in the highly turbid system of the Mazoe and the Luangwa rivers up to 13 351 ppm in the Shire River (Fig. 4d). While mean values of the two large reservoirs on the Zambezi River indicate undersaturated CO_2 conditions, overall mean pCO_2 of the much smaller Itezhi Tezhi Reservoir (1174 ppm), well above atmospheric equilibrium, was similar to the level of the two turbid river systems (Fig. 4d).

BGD
11, 16391–16445, 2014

Spatial variability and temporal dynamics of GHG concentrations and fluxes along the Zambezi River

C. R. Teodoru et al.

3.2 Temporal and spatial variability of CH_4

CH_4 along the Zambezi also showed a relatively large spatial heterogeneity, but low temporal variability (Fig. 4a). Lowest CH_4 concentrations during the two wet season campaigns (2012 and 2013) of 7 and 13 $nmol\,L^{-1}$, respectively, were both recorded at station ZBZ.9 immediately below the Victoria Falls. Highest value of the wet season 2012 campaign of 2394 $nmol\,L^{-1}$ was measured at ZBZ.17 while highest CH_4 concentration of the wet season 2013 of 12 127 $nmol\,L^{-1}$ was recorded at station ZBZ.5, downstream of the Barotse Floodplain (Fig. 4a). Mean value of the 2012 wet season campaign of 623 $nmol\,L^{-1}$ was 2 fold lower than mean CH_4 of the 2013 wet season (1216 $nmol\,L^{-1}$), and statistical analyses (paired t test at 0.05 level, $p > 0.516$, $n = 15$) suggest no significantly interannual variability. In the absence of comparative measurements at station ZBZ.9 below the Victoria Falls, lowest CH_4 concentration along the Zambezi during dry season 2013 campaign of 25 $nmol\,L^{-1}$ was recorded at ZBZ.10 in the Kariba Gorge (4 km downstream of the Kariba Dam), whereas maximum value of 874 $nmol\,L^{-1}$ was measured at ZBZ.5, downstream the Barotse Floodplains (Fig. 4a). Although mean CH_4 of the dry season 2013 of 361 $nmol\,L^{-1}$ was much lower than the equivalent mean of the wet season 2013 campaign, its median value of 305 $nmol\,L^{-1}$ and the paired t test ($p > 0.368$, $n = 8$) indicate little seasonality of CH_4 along the Zambezi River. CH_4 concentrations in the surface water of the two reservoirs on the Zambezi were generally lower compared to the riverine values (Fig. 4a). Concentrations in the Kariba were higher during wet season 2012 (mean 149 $nmol\,L^{-1}$) compared to the wet season 2013 (mean 28 $nmol\,L^{-1}$) but opposite in the Cahora Bassa (mean 54 and 78 $nmol\,L^{-1}$, respectively). The only CH_4 measurement in the Kariba Reservoir during dry season 2013 reached 19 $nmol\,L^{-1}$ (Fig. 4a).

Relatively low temporal variability of CH_4 (both interannual and seasonal) was also observed along the Kafue River (Fig. 4b), where concentrations varied from minimum 30, 100, and 92 $nmol\,L^{-1}$ during wet seasons 2012 and 2013, and the dry season 2013, respectively (all recorded at KAF.6, immediately below the Itezhi Tezhi Dam) to max-

BGD
11, 16391–16445, 2014

imum 992 nmol L^{-1} in the Kafue Flats (KAF.8) during 2012 wet season, and 550 and 898 nmol L^{-1}, respectively, at the lower edge of the flats (KAF.9) during 2013, both wet and dry seasons. With mean CH_4 values of 405, 329, and 416 nmol L^{-1} (or median 298, 302, and 274 nmol L^{-1}) for the wet seasons 2012 and 2013, and the dry season 2013, respectively, CH_4 concentrations along the Kafue were not statistically different during the wet season 2012 compared to 2013 the wet season 2013 (paired t test, $p > 0.541$, $n = 9$), nor during 2013 wet and dry seasons ($p > 0.543$, $n = 7$). CH_4 concentrations in the surface water of the Ithezhi Tezhi Reservoir were generally lower than riverine values, ranging between 37 and 89 nmol L^{-1} (mean 62 nmol L^{-1}) during wet season 2012, and 22 and 51 nmol L^{-1} (mean 40 nmol L^{-1}) during wet season 2013 (Fig. 4b). The only CH_4 measurement during 2013 dry season in the Itezhi Tezhi Reservoir (ITT.2) reached 71 nmol L^{-1}.

There was an overall positive, albeit week ($r^2 = 0.186$, $n = 106$) correlation between CH_4 and pCO_2 (log-log scale) for all rivers, tributaries and reservoirs, and all campaigns, with values at the lowest end mostly characteristic for the Kariba and Cahora Bassa reservoirs, and higher end occupied by the Shire River and several stations on the Zambezi and Kafue rivers located in-, or downstream of major floodplains/wetlands (Fig. 4c). With an average value of 769 nmol L^{-1} over the entire sampled period, CH_4 of the Zambezi River was twice as high as the average CH_4 concentration of the Kafue River (mean 381 nmol L^{-1}) (Fig. 4d). With the exception of the Shire River which displayed extremely high concentration (mean 19 328 nmol L^{-1} based on only 2 measurements), all other tributaries of the Zambezi River had similar mean CH_4 level ranging from 200 nmol L^{-1} in the highly turbid Luangwa River up to 514 nmol L^{-1} in the Lunsemfwa River (tributary of Luangwa) (Fig. 4d). CH_4 concentrations of all three reservoirs were comparable (mean 87, 66 and 54 nmol L^{-1} for Kariba, Cahora Bassa and Itezhi Tezhi, respectively) but consistently lower then riverine values (Fig. 4d).

BGD
11, 16391–16445, 2014

3.3 Temporal and spatial variability of N_2O

Consistent with the observed variability of pCO_2 and CH_4, N_2O in the Zambezi River was also highly variable both spatially and temporally (Fig. 5a). During both 2012 and 2013 wet season campaigns, N_2O along the Zambezi ranged from 4.1 $nmol\,L^{-1}$ (at ZBZ.5 downstream of the Barotse Floodplain) and 2.9 $nmol\,L^{-1}$ (at ZBZ.18, downstream the confluence with the Shire River) up to 8.5 and 8.0 $nmol\,L^{-1}$, respectively, both at ZBZ.11, downstream of the Kariba Dam (Fig. 5a). Higher overall concentrations but lower spatial variability was recorded during the dry season 2013, when concentrations ranged between 7.9 $nmol\,L^{-1}$ at ZBZ.13 (upstream of the Cahora Bassa Reservoir) and 11.4 $nmol\,L^{-1}$ downstream of the Kariba Dam (at ZBZ.10) (Fig. 5a). Statistical analyses of N_2O concentrations of the two wet season campaigns (mean 6.7, and 6.1 $nmol\,L^{-1}$ for 2012 and 2013, respectively) and the dry season 2013 (mean 8.8 $nmol\,L^{-1}$) suggest low interannual variability (paired t test, $p > 0.142$, $n = 15$) but strong N_2O seasonality (paired t test, $p < 0.0004$, $n = 8$) along the Zambezi River mainstem. The only measurement during the dry season 2013 in the surface water of the Kariba Reservoir suggest that N_2O was also higher (mean 8.6 $nmol\,L^{-1}$) compared to values of wet seasons 2012 and 2013 (mean 6.3 and 6.5 $nmol\,L^{-1}$, respectively). The same high spatial heterogeneity and low N_2O interannual variability was observed along the Kafue River, where values of the 2012 and 2013 wet seasons (mean 5.9 and 5.7 $nmol\,L^{-1}$, respectively) were not statistically different at 0.05 level (paired t test, $p > 0.549$, $n = 9$). It is worth noting that both minimum N_2O values of the two consecutive wet season campaigns were recorded at station KAF.8 in the Kafue Flats. Consistently higher and ranging from 7.0 $nmol\,L^{-1}$ in the Kafue Flats to 10.3 $nmol\,L^{-1}$ at the headwater station (KAF.1), N_2O during the dry season 2013 (mean 8.4 $nmol\,L^{-1}$) was significantly higher at 0.05 level (paired t test, $p < 0.001$, $n = 7$) compared to the 2013 wet season. N_2O in the surface water of the Itezhi Tezhi Reservoir were similar during both wet season campaigns (mean 6.8 and 6.5 $nmol\,L^{-1}$, respectively) and

BGD
11, 16391–16445, 2014

slightly higher than riverine values. The only one N_2O measurement in the Itezhi Tezhi during dry season 2013 (at ITT.2) reached 7.8 nmol L^{-1} (Fig. 5b).

There was an overall good ($r^2 = 0.48$) and negative correlation between N_2O and pCO_2 (Fig. 5c), with high N_2O concentrations and low pCO_2 mostly characteristic for reservoirs samples and riverine stations downstream of dams while low N_2O and high pCO_2 were characteristic for the Shire River and stations on the Zambezi and Kafue downstream of floodplains. There was no correlation between N_2O and NH_4^+ nor NO_3^-, while a positive relation with %DO applies only during wet seasons (data not shown). Despite seasonal and longitudinal variations, mean N_2O values were relatively similar among all sampled tributaries with little variability (from mean 6.2 nmol L^{-1} for Lunga to 7.5 nmol L^{-1} for Lunsemfwa) around grand mean of 6.9 nmol L^{-1}, with the exception of the Shire River characterized by distinct lower value (mean 2.7 nmol L^{-1}) (Fig. 5d). N_2O in the surface water of the Kariba and the Cahora Bassa reservoirs (mean 6.8 and 7.3 nmol L^{-1}, respectively) were close to riverine values (Fig. 5d).

4 Discussion

4.1 Patterns in GHG dynamics along the river continuum

As shown above, dissolved GHG concentrations along the Zambezi and the Kafue rivers display large spatial heterogeneity. Yet, concentrations followed similar longitudinal patterns during both consecutive wet season campaigns and only slightly different during dry season (mostly CO_2), which can be attributed to the connectivity between river and floodplains/wetlands, the input from major tributaries, and the presence of natural or anthropogenic barriers (waterfalls/rapids and reservoirs) along the aquatic continuum. We will examine these patterns in detail, using the example of pCO_2 during the 2012 wet season campaign since this represents the most complete dataset (Fig. 3a).

BGD
11, 16391–16445, 2014

Staring at an initial 1055 ppm at the Zambezi source (ZBZ.1), pCO_2 increased downstream to about 2450 ppm at ZBZ.2 as the river traverses a low gradient area, receiving water from the Chifumage and Luena tributaries which drain large floodplains in SE Angola. After a small decrease to 1970 ppm downstream of the confluence with the Kabompo River (ZBZ.3), pCO_2 increased sharply to over 7650 ppm at ZBZ.5 (ZBZ.4 was not sampled during wet season) as the river exchange waters with the Barotse Floodplains. This high CO_2 load, associated with low pH (6.97) and %DO (47 %) (Supplement, Table S1), was rapidly outgassed downstream due to a sharper gradient of this river sector that forms several rapids and the 14 m height Nygone Falls, reaching only 1980 ppm at ZBZ.6. Further downstream, pCO_2 peaked again reaching over 6300 ppm at ZBZ.7 as the river passes though the Caprivi-Chobe Swamps but dropped quickly down to 2500 ppm upstream of the Victoria Falls (ZBZ.8) due to the further steepening of the river gradient and the enhanced turbulent flow over the Mambova and the Katombora Rapids. As the river plunged down over 100 m height of the Victoria Falls, there was an instant and almost complete CO_2 outgassing, with river waters approaching atmospheric equilibrium at ZBZ.9 at the base of the fall (642 ppm). Downstream of the Victorial Falls, the river experiences a turbulent flow through the narrow, 100 km long Batoka Gorge and the Chimba Rapids, and CO_2 is expected to decrease further reaching values close to atmospheric concentrations at the Kariba Reservoir inflow. These CO_2-depleted inflow waters combined with CO_2 uptake by primary production (mean P rate $\sim$ 16.6 µmol C L^{-1} h^{-1}) could be put forward to explain the CO_2 under-saturated conditions encountered in the surface waters of the Kariba Reservoirs throughout all campaigns (Fig. 3a). In contrast to the CO_2 undersaturated epilimnetic conditions of the Kariba Reservoir, pCO_2 measured 70 km downstream of the Kariba Dam (at ZBZ. 11) of over 2000 ppm indicates the discharge of hypolimnetic, low DO and CO_2-loaded waters from the reservoir, formed as a result of thermal stratification of the water column (Kunz et al., 2011a). Riverine pCO_2 decreased further downstream the dam through the exchange with atmosphere, favored by the substantial broadening of the river sector, reaching 1230 ppm at ZBZ.12 and 890 ppm at ZBZ.13. pCO_2 in the

BGD
11, 16391–16445, 2014

surface water of the Cahora Bassa Reservoir were also below atmospheric equilibrium (168 and 342 ppm) and generally similar to those measured in the Kariba. As in the case of Kariba, pCO_2 level measured 40 km downstream of the Cahora Bassa dam (at ZBZ.14) of 1800 ppm indicates the discharge of hypolimnetic water through the bottom intake with high CO_2 content. pCO_2 decreased further downstream the dam due to the turbulent flow throughout the narrow Cahora Bassa Gorge and the broadening of the river section towards the coastal plains reaching 815 and 560 ppm at ZBZ.15 and ZBZ.16, respectively. Further downstream, pCO_2 increased again up to 1205 ppm (at ZBZ.17), most probably influenced by the wide riparian wetlands/marshes along the river banks, and increased further downstream to over 8180 ppm at ZBZ.17 as the Zambezi River receives waters from the highly loaded Shire River (12 700 ppm CO_2, 17.3 % DO) that drains a stagnant water complex of swamp/marshes (known as the Elephant Marsh). This high CO_2 load was slowly exchanged with the atmosphere towards the delta with river pCO_2 reaching 1790 ppm at ZBZ.19 and 1610 ppm at ZBZ.20 close to the river mouth (Fig. 3a).

This longitudinal pattern of pCO_2 along the Zambezi River described above was closely repeated during the second wet season campaign (2013) (Fig. 3a). Despite the overall lower values during the dry season 2013, pCO_2 followed also a relatively similar pattern reflecting also the influence of the Barotse Floodplains (even less pronounced), the quick CO_2 outgassing downstream due to the presence of several rapids and the Nygone Falls as well as the influence of the Chobe Swamps (Fig. 3a). The only obvious difference relative to the wet seasons occurred in the Zambezi headwaters when pCO_2 decreased substantially between the source station ZBZ.1 and ZBZ.2 compared to the increased pattern observed during both wet seasons. This could be potentially explained by the reduction of lateral input load as a result of loss of connectivity between the river and the riparian wetlands associated with lower water level during dry season. Similar longitudinal pattern reflecting the clear influence of wetlands, reservoirs, waterfalls/rapids along the Zambezi mainstem were also observed for CH_4 (Fig. 4a) as well as for N_2O, despite the latter showing a mirror image of the patterns in pCO_2

(Fig. 5a). The positive relationship between CH_4 and CO_2 suggest that both are largely controlled by organic matter degradation processes. The negative relationship between N_2O and pCO_2 and the positive relationship between N_2O and %DO suggest, on the other hand, that N_2O is removed by denitrification in the sediments. Low N_2O levels have been also observed in the Amazon floodplains (Richey et al., 1988) and in the hypolimnion of anoxic lakes (Mengis et al., 1997).

The influence of wetlands/floodplains and reservoirs on the dynamics of $p\text{CO}_2$ can be also seen along the Kafue River (Fig. 3b) where a steady increase in $p\text{CO}_2$ values was recorded during both wet seasons (2012 and 2013) at station KAF.4 below the Lukanga Swamps as well as in-, and downstream of the Kafue Flats (KAF.7, KAF.8, KAF.9) (Fig. 3b). The different pattern (decrease instead of increase) during the dry season 2013 for the upper Kafue (upstream of the Itezhi Tezhi Reservoir) can be explained by the loss of connectivity between river mainstem and the swamps. Low water levels during dry season 2013 which partially exposed the river bedrock along this stretch enhanced the turbulent flow (and subsequently the gas exchange coefficient) as suggested by oversaturated DO value (143 %), lowering the $p\text{CO}_2$ level close to atmospheric equilibrium. In the absence of an important lateral CO_2 source, photosynthetic CO_2 uptake by primary production higher than in the Kariba Reservoir ($P \sim 21.8\,\mu\text{mol C L}^{-1}\,\text{h}^{-1}$) should have further reduced the CO_2 down to undersaturated conditions. The peculiar situation downstream of the Itezhi Tezhi Reservoir where $p\text{CO}_2$ showed an increase in-, and downstream of the Kafue Flats also during 2013 dry season campaign can be explained by the specific hydrology of the flats altered by the operation of the two bordering dams. The completion of the Kafue Gorge Dam in 1972 led to an average rise in water table of over 2 m in the lower Kafue Flats which created a permanently flooded area of over 800 km^2 (McCartney and Houghton-Carr, 1998). Completed in 1978 with the purpose of upstream storage in order to ensure constant water supply for the Kafue Gorge Dam, the Itezhi Tezhi further altered the hydrology of the Kafue Flats. Triggered by rising energy demands, flows at the Itezhi Tezhi Dam have increased substantially during dry seasons while flood peaks have partly been delayed and attenuated, changing the timing and extent of flooding in the Kafue Flats (Mumba and Thompson, 2005). These hydrological alteration due to river damming and the creation of permanent flooded areas within the Kafue Flats may explain these high riverine pCO_2 levels in the Kafue Flats measured also during dry season 2013 (Fig. 3b). In contrast to the Zambezi River where riverine CO_2 concentrations downstream both dams were significantly higher compared to those in the surface water of its reservoirs, pCO_2 at KAF.6, immediately downstream the dam, were similar with those measured in the epilimnion of the Itezhi Tezhi Reservoir (Fig. 3b). Unlike Kariba and Cahora Bassa, the Itezhi Tezhi Dam was not designed for power production, water being released from the epilimnion over the spillways, with rare bottom water withdrawals only during low storage (Zurbrügg et al., 2012). As for the Kafue Gorge Reservoir, since no measurements were carried out in-, or immediately below the dam, we can only speculate the existence of a large CO_2 pool in the hypolimnion of the reservoir and the release to the river downstream of large amounts of GHGs. We can further expect that much lower pCO_2 levels measured consistently at KAF.10 (65 km downstream of the dam) compared to upstream stations (Fig. 3b) are the effect of rapid outgassing through the narrow and steep (600 m drop over 30 km) Kafue Gorge. All above mentioned effects of wetlands, reservoirs and the distinct hydrology on the dynamics of CO_2 concentrations along the Kafue River can also explain the longitudinal patterns of CH_4 and N_2O, and in combination with the hydrological conditions which determine the degree of water exchange with floodplains, are responsible for part of their temporal variability (Fig. 4b and c).

pCO_2 of all our sampled rivers and streams were generally well above atmospheric concentrations and comparable with pCO_2 values observed in other African rivers (i.e. Tendo, Aby, Oubangui, Tana, Athi-Galana-Sabaki rivers, Koné et al., 2009; Bouillon et al., 2009, 2014; Tamooh et al., 2013; Marwick et al., 2014). However, values were well below global levels of tropical rivers and streams given by Aufdenkampe et al. (2011) (median 3600 and 4300 ppm, respectively), except for the Shire River (mean and median 13 350 ppm, $n = 2$) (Fig. 3d). With pCO_2 in the surface water

BGD
11, 16391–16445, 2014

of the Itezhi Tezhi Reservoir above atmospheric concentration (mean 1174, median 1127 ppm), and substantially higher than both Kariba (mean 267, median 275 ppm) and Cahora Bassa reservoirs (mean 219, median 192 ppm), its level was still lower than literature-based median value for tropical lakes and reservoirs of 1900 ppm suggested by Aufdenkampe et al. (2011) (Fig. 3d). Undersaturated CO_2 conditions in surface waters such as of the Kafue and the Cahora Bassa reservoirs have being previously described for other reservoirs in Africa (Bouillon et al., 2009; Tamooh et al., 2013). Overall CH_4 concentrations in the Zambezi River mainstem (mean 769 $nmol\,L^{-1}$), higher than those of its major tributaries and reservoirs (Fig. 4d) were on average much higher than those measured in other African river systems such as the Oubangui River (~ 160 $nmol\,L^{-1}$, Bouillon et al., 2014), the Tana River (~ 160 $nmol\,L^{-1}$, Bouillon et al., 2009), the Galana River and several steams in Kenya (250 and 180 $nmol\,L^{-1}$, respectively, Marwick et al., 2014), and three rivers in Ivory Coast (Comoé: 206 $nmol\,L^{-1}$, Bia: 238 $nmol\,L^{-1}$, and Tanoé: 345 $nmol\,L^{-1}$, Koné et al., 2010). A comparable range was also observed in tributaries of the Oubangui (~ 740 $nmol\,L^{-1}$, Bouillon et al., 2014) and in the Athi-Galana-Sabaki River system in Kenya (~ 790 $nmol\,L^{-1}$, Marwick et al., 2014). With the exception of the Shire River where low N_2O concentrations of ~ 2.7 $nmol\,L^{-1}$ could be explained by denitrification, mean N_2O range in the Zambezi River Basin (6.2–7.5 $nmol\,L^{-1}$, Fig. 5d) was similar to those of the Oubangui River mainstem and its tributaries (7.5 and 9.9 $nmol\,L^{-1}$, respectively, Bouillon et al., 2009). However, locally elevated concentrations linked to high anthropogenic N inputs have been recorded in the Athi-Galana-Sabaki River system in Kenya (up to 26 $nmol\,L^{-1}$, Marwick et al., 2014).

4.2 Dissolved inorganic carbon and its stable isotope signature

DIC in freshwater can be differentiated into two fractions with distinct origins and behaviors: carbonate alkalinity, mostly in the form of bicarbonate ions (HCO_3^-) which comes from soil and bedrock weathering, and dissolved CO_2, which results from respiration

BGD
11, 16391–16445, 2014

in soils, groundwaters, river sediments and waters column (Meybeck, 1987; Amiotte-Suchet et al., 1999). As the relative proportion of the two DIC fractions (and concentrations) depends greatly on the lithology of the drainage basin, rivers draining carbonate-rich watersheds would typically have high DIC concentrations (well above 1 $mmol L^{-1}$) of which HCO_3^- represents the major fraction compared to dissolved CO_2 (Meybeck, 1987). In these hard waters, characterized by high pH and high conductivity, HCO_3^- contributes to the majority of the TA. In contrast, rivers draining non-carbonate rocks and/or soils with high organic content would have lower DIC concentrations (well below 1 $mmol L^{-1}$), of which dissolved CO_2 commonly represents the dominant fraction (Abril et al., 2014b). Characterized by low pH and low conductivity, these acidic, organic rich waters (soft waters) generally contain high DOC levels, sometimes exceeding DIC concentrations (Rantakari and Kortelainen, 2008; Whitfield et al., 2009; Einola et al., 2011), and organic acid anions contribute impornantly to the TA (Driscoll et al., 1989; Hemond, 1990; Hunt et al., 2011).

The DIC values in all our sampled rivers (mean 1.32 $mmol L^{-1}$) together with conductivity (mean 140.1 $\mu S cm^{-1}$) and pH values (mean 7.61) may suggest the carbonate-rich lithology of the basin. However, low DIC, pH and conductivity values in the headwaters and their increasing patterns downstream along both the Zambezi and the Kafue rivers during all campaigns (data in the Supplement) suggest either different chemical weathering rates or/and that a proportion of HCO_3^- may also come from silicate rock weathering. This is also suggested by the overall good correlation of TA with the sum of Ca^{2+} and Mg^{2+} ($r^2 = 0.84$, Fig. 6a) and the rather weak relationship ($r^2 = 0.18$) with DSi (Fig. 6b). To distinguish between the contribution of silicate and carbonate weathering to the HCO_3^-, we applied the simple stoichiometric model of Garrels and Mackenzie (1971) which calculates the contribution of carbonate weathering (TA_{carb}) to TA from Ca^{2+} and Mg^{2+}, and the contribution of silicate weathering (TA_{sil}) to TA from

BGD
11, 16391–16445, 2014

DSi according to:

$$TA_{carb} = 2 \times \left([Ca^{2+}] + [Mg^{2+}] - [SO_4^{2-}] \right) \quad \text{(R1)}$$

$$TA_{sil} = [DSi]/2 \quad \text{(R2)}$$

While SO_4^{2-} in Reaction (R1) allows to account for Ca^{2+} originating from dissolution of gypsum ($CaSO_4$), its contribution was ignored due to the absence of SO_4^{2-} measurements. However, occurrence of gypsum in the Zambezi Basin is sporadic and mostly as nodules in a clay-rich dambo within the Kafue Flats (Briggs and Mitchell, 1991), and in the upper catchment of Shire River (downstream of Lake Malawi) (Ashton at al., 2001).

Results indicate significant, and positive regression between the modeled TA ($TA_{Carb}+TA_{Sil}$) and observed TA ($r^2 = 0.87$, $n = 103$) for all measured tributaries, reservoirs and Zambezi mainstem samples with most of the data points falling on the 1 : 1 line (Fig. 7a). Exception from this pattern is found on the upper most two sites of the Kafue River (KAF.1 and KAF.2) during 2013 dry campaign where modeled TA is twice as high as the observed TA (Fig. 7a) due to unusually high both Ca^{2+} (1860 and 1360 µM) and Mg^{2+} (1035 and 1247 µM). Such high value during low flow period, also linked to low pH (around 6) and low conductivity (5.4 and 32.6 $\mu S\,cm^{-1}$, respectively), found in this area of intense mining activities (mostly copper and cobalt) could be the result of effluent discharge from the processing plants or leaking of contaminated water from the extraction pits, tailings and slag dumps. The contribution of carbonate rock weathering estimated as the percentage of TA_{Carb} (%TA_{Carb}) to the total modeled TA ($TA_{Carb}+TA_{Sil}$) in all samples ranged between 28 and 97 % (mean 88 %) (Fig. 7b). Highest TA_{Carb} contribution was found for reservoirs (min. 86 %, max. 96 %, mean 91 %) and tributaries (min. 64 %, max. 97 %, mean 90 %) while largest range (min. 29 %, max. 93 %, mean 84 %) was found for the Zambezi River mainstem (Fig. 7b). Minimum TA_{Carb} value of only 29 % correspond to the Zambezi source sample (ZBZ.1) during 2013 dry campaign (Fig. 7b). The strong ($r^2 = 0.88$), positive, exponential relationship between %TA_{Carb} and TA (Fig. 7b) and the general increased %TA_{Carb} along the Zambezi main-

BGD
11, 16391–16445, 2014

Spatial variability and temporal dynamics of GHG concentrations and fluxes along the Zambezi River

C. R. Teodoru et al.

stem (data not shown) may indicate lower contribution of carbonate rock weathering in the more humid forest areas of the northwestern basin compared to the mostly open grassland areas and savannah in the south and towards the ocean.

$\delta^{13}C_{DIC}$ in aquatic systems varies over a large range, being primarily controlled by both in-stream and watershed processes (Finlay and Kendall, 2007). C reservoirs which act as a source of riverine DIC such as atmosphere, bedrocks, groundwater or soil have distinct isotopic signatures. Marine carbonates rocks have a $\delta^{13}C$ close to 0 ‰ whereas $\delta^{13}C$ of atmospheric CO_2 is about −7.5 ‰ (Mook et al., 1983). The $\delta^{13}C_{DIC}$ of soil CO_2 depends on the plant photosynthetic pathways and the source of the organic matter such as that systems where soil CO_2 involved in weathering comes primarily from decomposition of plant organic matter will have a $\delta^{13}C_{DIC}$ signature close to the signature of the initial substrate (i.e. −34 to −22 ‰ in the case of C3 plants and −16 and −9 ‰ in the case of C4 plants, Vogel, 1993; Finlay and Kendall, 2007). While in-stream CO_2 uptake during aquatic primary production and degassing of CO_2 along the river course (that generates an isotopic equilibration with the atmosphere), make $\delta^{13}C_{DIC}$ less negative, the addition of respired CO_2 (with isotopic signature similar with the organic C substrate) and the increasing contribution of HCO_3^- (compared to CO_2) lowers the $\delta^{13}C_{DIC}$ (Finlay and Kendall, 2007). The overall $\delta^{13}C_{DIC}$ values in all our samples ranged from −21.9 ‰ at the Zambezi source (during 2013 dry season campaign) to −1.8 ‰ in the Kariba and the Cahorra Bassa reservoirs (during 2013 wet season), suggesting the occurrence of various C sources as well as in-stream processes. The overall average value of −7.3 ‰ and the good relationship between $\delta^{13}C_{DIC}$ and DSi : Ca^{2+} molar ratio which explains 88 % of the variability in $\delta^{13}C_{DIC}$ suggest the relative importance of carbonate to silicate mineral weathering (Fig. 7c). However, the increase in $\delta^{13}C_{DIC}$ along the Zambezi mainstem (Fig. 7d) alongside with an increase in POC in the lower Zambezi (data not shown) points out to the interplay between downstream degassing and the degradation of laterally derived organic matter in controlling $\delta^{13}C_{DIC}$ along the Zambezi River. The importance of these processes on riverine $\delta^{13}C_{DIC}$ has been previously observed for other African rivers (Tamooh et al., 2013; Bouillon at al., 2014).

A clear and instant effect of degassing with a fast enrichment in $\delta^{13}C_{DIC}$ of the remaining DIC pool, and explained by the isotopically depleted CO_2 fraction relative to HCO_3^- and CO_3^{2-} (Doctor et al., 2008), can be best seen at the Victoria Falls where during 2012 wet campaign we noticed a rapid increase in $\delta^{13}C_{DIC}$ from −8.5 to −6.9 ‰ (Fig. 7d) correlated with an instant decrease in pCO_2 from 2500 to 640 ppm (Fig. 3a). Similar CO_2 degassing effects on $\delta^{13}C_{DIC}$ were observed also downstream of the Barotse Floodplains (ZBZ.5 to ZBZ.6, 195 km) and downstream of the Chobe Swamps (ZBZ.7 to ZBZ.8, 74 km, see map) where, during the same 2012 wet campaign, the drop in pCO_2 from 7560 to 1890 ppm and 6307 to 2500 ppm, respectively, was accompanied by an enrichment in $\delta^{13}C_{DIC}$ from −8.5 to −6.9 ‰ and from −7.0 to −6.2 ‰, respectively (Figs. 3a and 7d). Ranging between −4.1 and −1.8 ‰ (mean −2.9 ‰), the $\delta^{13}C_{DIC}$ values in the surface waters of the Kariba and the Cahora Bassa reservoirs were highest among all samples during all three campaigns (Fig. 7d). Associated with mostly undersaturated CO_2 conditions and negative CO_2 fluxes (Figs. 3a and 9a), R rates (in the order of $\sim 0.8\,\mu mol\,C\,L^{-1}\,h^{-1}$) not different than riverine values, and P rates ($\sim 25.0\,\mu mol\,C\,L^{-1}\,h^{-1}$) twice as low as river values, the higher $\delta^{13}C_{DIC}$ values found in both reservoirs on the Zambezi can be primarily explained by the atmospheric CO_2 uptake during primary production, a process capable of generating strong diel variations (Parker et al., 2005). Slightly lower $\delta^{13}C_{DIC}$ values (−7.1 to −3.0 ‰, mean −5.2 ‰) characterized the surface water of the Itezhi Tezhi Reservoir on the Kafue River. The observed $\delta^{13}C_{DIC}$ enrichment in the Itezhi Tezhi with increasing distance from the river inflow correlated with a gradual decrease in pCO_2, and comparable R rates ($\sim 0.7\,\mu mol\,C\,L^{-1}\,h^{-1}$) but higher P ($\sim 48.4\,\mu mol\,L^{-1}\,h^{-1}$) suggest the combined effect of P and CO_2 evasion (mostly originating with river inflow). While $\delta^{13}C_{DIC}$ in the Kafue River (−7.3 ± 1.7 ‰, $n = 26$, excluding the Itezhi Tezhi Reservoir) was not significantly different from that of the Zambezi mainstem (−7.7 ± 3.6 ‰, $n = 42$, exclud-

BGD
11, 16391–16445, 2014

ing the Kariba and the Cahora Bassa reservoirs), $\delta^{13}C_{DIC}$ values of smaller tributaries were significantly lower. The $\delta^{13}C_{DIC}$ values of the Kabompo (−10.7 ± 0.7 ‰, $n = 3$), Lunga (−9.8 ± 1.0 ‰, $n = 5$), Luangwa (−9.4 ± 1.0 ‰, $n = 8$), Lunsemfwa (−8.9 ± 1.7 ‰, $n = 4$) and Mazoe tributaries (−9.4 ‰, $n = 1$) would suggest that in addition to carbonate weathering, there is a substantial increased contribution of soil CO_2 from C4 vegetation. Intermediate $\delta^{13}C_{DIC}$ values between reservoirs and tributaries were measured in the Shire River (−5.1 ± 2.4 ‰, $n = 2$) which drains the soft-water Lake Malawi. These isotopically enriched $\delta^{13}C_{DIC}$ values there coupled with highest recorded pCO_2 concentrations (mean 13 350 ppm, Fig. 3d) must be explained by exceptionally high CO_2 degassing rates of over 23 000 mg C m^{-2} d^{-1}, up to one order of magnitude larger than all other measured fluxes (Fig. 9a).

4.3 Diurnal variation in GHG concentrations

To account for the importance of diel fluctuation on the investigated biogeochemical parameters, we performed a 24 h sampling campaign at station ZBZ.11 on the Zambezi River between 22 and 23 November 2013 (dry season). Measurements suggest a small variation of barometric pressure (0.6 kPa), and a small gradual increase in temperature (of 0.7 °C) from midday to midnight follow by a decrease (of 0.6 °C) between midnight and 9 a.m. when temperature start rising again (Fig. 8a and b). Similar sinusoidal patterns were observed over the same time period for DO (increased saturation with 7 %, decreased with 5 % followed by increase), pH (increased from 6.95 to 7.32, decrease to 7.21 followed by increase), and $\delta^{13}C_{DIC}$ (increased from −6.4 to −5.5 ‰, decrease to −6.1 ‰ followed by increase) (Fig. 8c–e). In contrast, a mirror-reverse pattern was recorded for pCO_2 which gradually decreased 30 % (from 1655 to 1180 ppm) from midday to midnight (∼ 40 ppm h^{-1}) and increased 30 % (up to 1430 ppm) until 9 a.m. (∼ 30 ppm h^{-1}), when values start slowly decreasing with the onset of primary production (Fig. 8g). Following pCO_2 pattern, DIC decreased 0.1 mmol L^{-1} (12 %) between 12 a.m. and 12 p.m., and increased 0.03 mmol L^{-1} (3 %) between 12 p.m. and 9 a.m.

BGD
11, 16391–16445, 2014

(Fig. 8f). While CH_4 followed the general pattern of pCO_2, decreasing and increasing both with approximately 50 % (decreased with 270 μmol L^{-1} and increased with 150 μmol L^{-1} or ~ 25 μmol L^{-1} h^{-1}), N_2O showed no distinct diurnal variations (Fig. 8h, i). While these patterns provide clear evidences of diel variations of physico-chemical parameters onset by the coupling between P and R, their overall influence on the river biogeochemistry seems to be rather small and unable to explain the observed large variability across the basin. As, for obvious logistics reasons, we have sampled exclusively during day time, based on the above discussed diel fluctuations, if anything, we may have possibly underestimated various parameters (i.e. dissolved gas concentrations and fluxes) by maximum 10 to 15 %. To our knowledge most existent studies which involved in situ measurements and data collection have been performed in the same manner, and are therefore subject to the same limitations.

4.4 CO_2 and CH_4 fluxes

Driven by supersaturation in CO_2 and CH_4 with respect to atmospheric equilibrium (Figs. 3 and 4), the Zambezi River and all sampled tributaries were net sources of CO_2 and CH_4 to the atmosphere. However, levels are well below the global emission range proposed by Aufdenkampe et al. (2011) and Bastviken et al. (2011) for tropical rivers and streams (Fig. 9a and b). Overall mean CO_2 and CH_4 fluxes of the Zambezi River of 3380 mg C m^{-2} d^{-1} (median 1409) and 48.5 mg C m^{-2} d^{-1} (median 12.4) were not different from those of its main tributary (the Kafue River) of 3711 mg C m^{-2} d^{-1} (median 1808) and 67.8 mg C m^{-2} d^{-1} (median 14.7) (Fig. 9). CO_2 fluxes along the Zambezi mainstem were generally lower during 2013 dry season (mean 623 mg C m^{-2} d^{-1}) compared to fluxes of the 2012 and 2013 wet season campaigns (mean 3280 and 5138 mg C m^{-2} d^{-1}, respectively). The opposite situation was observed for CH_4 where measured fluxes during 2013 wet campaign (no CH_4 fluxes were measured during 2012 wet season) (mean 26.5 mg C m^{-2} d^{-1}) were significantly lower compared to the 2013 dry season (mean 92.7 mg C m^{-2} d^{-1}). Singular events of negative CO_2 fluxes

BGD
11, 16391–16445, 2014

on the Zambezi mainstem were measured only during 2013 dry season campaign at ZBZ.6 and ZBZ. 13 (mean −23 and −33 $mg C m^{-2} d^{-1}$, respectively), and corresponded to riverine pCO_2 values of 300 and 421 ppm, respectively (Fig. 3a). Similar situation of undersaturated riverine CO_2 level was encountered also on the Kafue River only during 2013 dry season (at KAF.4, 330 ppm, Fig. 3b) but no reliable flux rate was determined there due to unusual, irregular fluctuations of CO_2 concentrations inside the floating chamber. With the exception of this, all other measured CO_2 fluxes on the Kafue River were positive, and fluxes of the dry season 2013 (mean 3338 $mg C m^{-2} d^{-1}$) were not significantly different from those of the two wet seasons (mean 2458 and 5355 $C m^{-2} d^{-1}$, respectively). As in the case of the Zambezi River, CH_4 fluxes along the Kafue were also higher during 2013 dry season (mean 149.5 $mg C m^{-2} d^{-1}$) compared to the 2013 wet season (mean 16.8 $mg C m^{-2} d^{-1}$). Chamber measurements provide the combined CH_4 flux resulting from both ebullitive and diffusive fluxes. Since CH_4 concentrations during the dry season were not higher compared to the wet season (Fig. 4a and b), the most likely explanation for the higher CH_4 rates during low water level observed along both Zambezi and Kafue rivers relates to higher contribution of ebullitive fluxes. This is consistent with higher CH_4 ebullitive fluxes during low waters than during high and falling waters in the Amazonian rivers (Sawakuchi et al., 2014). Higher contribution of ebbulition during 2013 dry campaign is further supported by the comparison between total CH_4 flux (measured with the floating chamber) and the estimated diffusive CH_4 flux (F) from the interfacial mass transfer mechanism from water to air expressed as:

$$F = k \cdot (C_w - C_{eq}) \tag{2}$$

where k is the gas transfer velocity back calculated from the measured CO_2 flux and normalized to a Schmitd number (Sc) of 600 ($k_{600} = k \cdot (600/Sc)^{-1/2}$), and C_w and C_{eq} are dissolved gas concentrations in the surface water and in the air, scaled by solubility to the value it would have when in the equilibrium with the atmosphere. Assuming that the difference between the computed (diffusive) and measured CH_4 flux is purely due

BGD
11, 16391–16445, 2014

to ebullition, the comparison suggests that on average, 73 % of measured CH_4 fluxes during the 2013 wet campaign along both the Zambezi and the Kafue river were due to diffusive processes and only 27 % originated from ebullition. In contrast, ebullition during the 2013 dry campaign accounted for up to 77 % of measured CH_4 fluxes. This is in agreement with the contribution of CH_4 ebullition of more than 50 % of total CH_4 emissions among different Amazonian rivers and seasons (Sawakuchi et al., 2014).

Gas transfer velocity values (k_{600}) ranging between 0.2 and 6.3 $cm\,h^{-1}$ (mean 2.7, median 2.3 $cm\,h^{-1}$) for the Zambezi River, from 0.4 to 7.9 $cm\,h^{-1}$ (mean 2.1, median 1.7 $cm\,h^{-1}$) for the Kafue River, and between 0.6 and 6.2 $cm\,h^{-1}$ (mean 3.1, median 3.4 $cm\,h^{-1}$) for all other tributaries are close to the k of ~ 3 $cm\,h^{-1}$ suggested by Cole and Caraco (2001) for large rivers but well below the median global values proposed by Aufdenkampe et al. (2011) for tropical rivers and streams (12.3 and 17.2 $cm\,h^{-1}$, respectively), and the basin-wide average value of 20.6 $cm\,h^{-1}$ for the Zambezi given by Raymond et al. (2013). Our few extreme k values (20.3 to 79.7 $cm\,h^{-1}$) obtained from the flux chamber measurements performed in static mode (non drift with the current) as a result of an additional turbulence induced by the water rushing against the chamber walls have been excluded from the overall calculations. In situ experiments designed to explore the effect of additionally induced turbulence by the chamber walls on the flux chamber measurements in rivers, and performed both on static mode at various water velocities and drift, suggest a clear, linear dependency of k on the velocity of water relative to the floating chamber (Cristian R. Teodoru, unpublished data). Such dependency, the culprit or potentially large overestimation of flux measurements in rivers, disserves further attention.

It is worth noting that the highest CO_2 fluxes along both Zambezi and Kafue rivers were found mostly in-, and downstream wetlands and floodplains (i.e. ~ 12 500 $mg\,C\,m^{-2}\,d^{-1}$, downstream of the Barotse Floodplains; > 4000 $mg\,C\,m^{-2}\,d^{-1}$ downstream of the Chobe Swamps; > 12 700 $mg\,C\,m^{-2}\,d^{-1}$ in-, and downstream of the Kafue Flats) and in the delta (> 10 000 $mg\,C\,m^{-2}\,d^{-1}$). Such high outgassing rates there are consistent with findings of studies on the Amazonian river-floodplains system which stress the importance of wetlands and floodplains on river biogeochemistry, especially on the CO_2 fluxes (Richey et al., 2002; Abril et al., 2014a). Moreover, the highest CO_2 and CH_4 fluxes of the Zambezi mainstem (> 20 000 and 154 mg C m^{-2} d^{-1}, respectively) were consistently measured at ZBZ.18 immediately downstream the confluence with the Shire River. The only outlet of Lake Malawi, the Shire River passes through a large stagnant waters complex of swamp/mashes (the Elephant Marsh) before it joins the Zambezi River. With mean CO_2 and CH_4 fluxes in the region of 23 100 and 1170 mg C m^{-2} d^{-1}, respectively, and way above the global emission level for tropical streams (Fig. 9), the Shire River represent a hotspot for both CO_2 and CH_4 emissions. Average CO_2 and CH_4 emissions for all tributaries (excluding the Kafue River) of 4790 mg C m^{-2} d^{-1} (median 2641) and 180.7 mg C m^{-2} d^{-1} (median 10.1), respectively, while higher than of the Zambezi mainstem, are still well below the global level for tropical rivers and streams (Fig. 9). In contrast, the two reservoirs on the Zambezi Rivers (the Kariba and the Cahora Bassa), were both sinks of atmospheric CO_2 (mean −141 and −356 mg C m^{-2} d^{-1}), but low sources of CH_4 (5.2 and 1.4 mg C m^{-2} d^{-1}, respectively) (Fig. 9). Different situation was encountered for the much smaller Itezhi Tezhi Reservoir on the Kafue River, where average CO_2 emission in the range of 737 mg C m^{-2} d^{-1} (median 644), approaches the global emission rate for tropical lakes and reservoirs (Fig. 9a) but CH_4 flux of 25.8 mg C m^{-2} d^{-1}, while highest among our sampled reservoirs, is still way below the global range (Fig. 9b). Combined average CO_2 and CH_4 fluxes of all reservoirs reach 202 mg C m^{-2} d^{-1} (median −77) and 13.5 mg C m^{-2} d^{-1} (median 1.3), respectively.

CH_4 emissions, even much lower in term of areal rate compared to their companion CO_2 fluxes as found for all our aquatic types, have equal or even higher importance in term global warming potential (GWP). Using the GWP factor of CH_4 of 86 CO_2-equivalent (CO_2eq) for 20 yr time horizon (IPCC, 2013), mean CH_4 fluxes of the Zambezi and Kafue rivers mainstem would translate into 4171 and 5830 mg C-CO_2eq m^{-2} d^{-1}, respectively, slightly higher but comparable with CO_2 fluxes (3380 and 3711 mg C m^{-2} d^{-1}, respectively). However, CH_4 emissions from tributaries (with-

BGD
11, 16391–16445, 2014

out Kafue) and reservoirs of 15 540 and 1160 mg C-CO_2eq m^{-2} d^{-1}, respectively, are distinctly higher, surpassing the CO_2 emissions by 3 and 6 fold, respectively.

The Victoria Falls on the upper Zambezi form another important hotspot for GHG emissions. A simple calculation suggests that the instant and almost complete degassing of CO_2 (75 %) and CH_4 (97 %) during 2013 wet season campaign as the water dropped over 108 m depth of the fall at a rate of 1245 m^3 s^{-1}, released daily into the atmosphere approximately 75 t C d^{-1} in form of CO_2 and 0.4 t C d^{-1} as CH_4. For CO_2, this is equivalent with what the Zambezi River would emit on average over an area of more than 20 km^2 or over a stretch of 33 km length for an average river width of 600 m.

There is a significant, exponential correlation between pCO$_2$ (ppm) and CO_2 flux (F_{CO_2} in mg C m^{-2} d^{-1}) which could be used to roughly estimate emission rates relying on river pCO$_2$ values only:

$$F_{CO_2} = -2770.6 + 3229.7 \times \mathrm{EXP}^{(0.00016 \cdot pCO_2)},\ r^2 = 0.75,\ n = 92 \tag{3}$$

However, this relation should be used with care in other river systems where additional calibrations must be performed, or for global flux estimates where a larger dataset of many rivers must be first considered.

4.5 C mass balance

We constructed a simple C mass balance over the study period for the Zambezi River which consists of three main components: (i) the outgassed load to the atmosphere, (ii) the C load to the sediment, and (iii) the C export load to the ocean (Fig. 10). The GHG load to the atmosphere was calculated as the product between surface area and the measured areal CO_2 and CH_4 fluxes. Surface area of rivers was estimated by mapping each river sector between two sampling points using the geometrical applications in Google Earth Pro. Each sector was then multiplied with the corresponding average flux of the two bordering sampling points and results were summed up to calculate the overall GHG load (in kt C yr^{-1}). Estimates of river surface area was restricted to the Zambezi mainstem (1879 km^2 without reservoirs) and the Kafue river (287 km^2 without reservoirs) (Table 1a) for which we have a relatively good longitudinag distribution of data, and where an extrapolation between sampling stations can be made with some confidence. Back calculated from the overall riverine CO_2 and CH_4 loads to the atmosphere divided by total river surface, these area weighted-average fluxes for the Zambezi River (4291 and 45.0 $mg\,C\,m^{-2}\,d^{-1}$, respectively) and the Kafue River (2962 and 20.0 $mg\,C\,m^{-2}\,d^{-1}$, respectively) (Table 1a) are slightly different (higher for the Zambezi and lower for the Kafue) than normal average fluxes. In the absence of reliable areal estimates for the rest of the hydrological network, fluxes of all other sampled tributaries, even potentially important, were not included in the overall emission calculation. GHG emissions for reservoirs were calculated as a product between the corresponding mean fluxes and surface area (Table 1a). Area of the Kariba (5364 km^2), Cahora Bassa (2670 km^2), Itezhi Tezhi (364 km^2) and Kafue Gorge (13 km^2) reservoirs were taken from literature (Beilfuss and dos Santos, 2001; Kunz et al., 2011a, b; Kling et al., 2014). CO_2 and CH_4 emissions for the Kafue Gorge Reservoir were extrapolated using mean fluxes of the Itezhi Tezhi Reservoir. C deposition component was estimated considering only removal in reservoirs while deposition in rivers, in the absence of direct measurements, was assumed negligible. C deposition in the Kariba and the Itezhi Tezhi reservoirs of 120 and 16 $kt\,C\,yr^{-1}$, respectively, were taken from available literature data (Kunz et al., 2011a, b) while C retention in the Cahora Bassa and the Kafue Gorge reservoirs of 60 and 0.6 $kt\,C\,yr^{-1}$, respectively, were extrapolated from the rates of the Kariba and the Itezhi Tezhi reservoirs (Table 1a). The export load to the ocean (Table 1b) was computed as the product between the annual flow rate (Q) and the average POC (2.6 $mg\,L^{-1}$), DOC (2.2 $mg\,L^{-1}$) (data in a companion paper) and DIC (30.8 $mg\,L^{-1}$) measured at the two stations in the delta, close to the river mouth (ZBZ.19 and ZBZ.20). Lacking direct discharge measurements at the river mouth over the study period, an annual average flow rate of 3779 $m^{-3}\,s^{-1}$ was calculated from the existing literature data of 3424 and 4134 $m^3\,s^{-1}$ (Beilfuss and dos Santos, 2001; World Bank, 2010).

BGD
11, 16391–16445, 2014

Mass balance calculations suggest a total C yield of 7215 $\mathrm{kt\,yr^{-1}}$ (or 5.2 $\mathrm{t\,C\,km^{-2}\,yr^{-1}}$) of which: (i) 38 % (2779 $\mathrm{kt\,C\,yr^{-1}}$) is annually emitted into the atmosphere, mostly in the form of CO_2 (98 %), (ii) 3 % (196 $\mathrm{kt\,C\,yr^{-1}}$) is removed by sedimentation in the main reservoirs, and (iii) 59 % (4240 $\mathrm{kt\,C\,yr^{-1}}$) is exported to the ocean, mostly in the form of DIC (87 %), with organic C component accounting only for a small fraction (7 % POC and 6 % DOC) (Fig. 10). Even potential large uncertainties for the overall balance may occur from the lack of direct discharge measurements at the river mouth, the limitation of riverine GHG emission only to the Zambezi mainstem and the Kafue river, and from missing data on C removal by sedimentation in rivers, the overall picture is rather consistent with previous figures of global C budgets (Cole et al., 2007; Battin et al., 2009). It is worth mentioning that our relatively lower C emissions component of the balance compared to global budgets, is the direct result of atmospheric CO_2 uptake by the surface waters of the Kariba and Cahora Bassa reservoirs (Table 1). Despite their relatively low uptake rates (−141 and −356 $\mathrm{mg\,C\,m^{-2}\,d^{-1}}$, respectively, Table 1), the huge areal extent of the two reservoirs, which accounts for more that 76 % of the total estimated aquatic surface, lowered the overall outgassed load by 20 %. This in turn, reduces the relative contribution of the C emission component of the balance by 6 %. In other words, if both reservoir on the Zambezi were C neutral (most likely C sources since the atmospheric CO_2 uptake must be compensated by rapid release of hypolimnetic CO_2 pool with the disruption of thermal stratification during the winter period in July–August), the relative contribution of emissions, deposition and export to the total budget would reach 43, 3, and 54 %, respectively. The influence of reservoirs on riverine C balance can be clearly seen in the case of Kafue River where a similar balance approach would suggest a reverse situation with emissions surpassing the downstream export by almost two fold. With both Itezhi Tezhi and Kafue Gorge reservoirs contributing 1/3 to the total emissions of 417 $\mathrm{kt\,C\,yr^{-1}}$ (Table 1a), a C burial rate of 17 $\mathrm{kt\,C\,yr^{-1}}$ (Table 1a) and an export load of around 258 $\mathrm{kt\,C\,yr^{-1}}$, this would translate into a similar C yield of 4.4 $\mathrm{t\,C\,km^{-2}\,yr^{-1}}$ (691 $\mathrm{kt\,yr^{-1}}$) but the balance between emission, deposition and export components would be shifted to 60, 3, and 37 %, respectively. Moreover, failing to in-

BGD
11, 16391–16445, 2014

corporate C emissions from the entire hydrological network of the Zambezi River basin clearly underestimates the overall C outgassing load. For instance, using a total rivers and streams area of 7325 km^2 for the Zambezi basin (excluding lakes and reservoirs) derived from a limnicity index of 0.42 % and a total catchment area of 1 729 941 km^2 (Raymond et al., 2013), and a mean CO_2 and CH_4 flux of 3630 and 32.5 $mg\,C\,m^{-2}\,d^{-1}$, respectively (average between Zambezi and Kafue values, Table 1a), GHG emission from the entire Zambezi River network would reach ~ 9780 $kt\,C\,yr^{-1}$. Taking further into account C emissions and sinks in reservoirs, and export to the ocean, a simple calculation would suggest a total C yield of ~ 13 710 $kt\,yr^{-1}$ (~ 10 $t\,C\,km^{-2}\,yr^{-1}$) of which GHG emissions account for up to 68 % while the export load represent less than 30 %. Moreover, the relative contribution of GHG to the present C budget would increase considerably if taking into account emissions from the highly productive systems such as wetlands and floodplains of which influence on the biogeochemistry of the river has been clearly demonstrated throughout this work and elsewhere (Aufdenkampe et al., 2011; Abril et al., 2014a). For instance, a rough estimate of C emissions from the only four major floodplain/wetlands in the basin (the Barotse Floodplain: 7700 km^2, the Chobe Swamps: 1500 km^2, the Lukanga Swamps: 2100 km^2, and the Kafue Flats: 6500 km^2) calculated using our fluxes measured on the river downstream of their locations, and applied to merely half of their reported surface area and over only the seasonal flooding period (half-year) would add to the overall emissions an extra 16 000 $kt\,C\,yr^{-1}$. Assuming no further C deposition in these areas, the incorporation of wetlands into the present budget would increase the total C yield to 17 $t\,C\,km^{-2}\,yr^{-1}$ (or 23 400 $kt\,C\,yr^{-1}$) while the relative contribution of degassing would reach 81 % (19 000 $kt\,C\,yr^{-1}$), lowering the contribution of C deposition and export to 1 and 18 %, respectively, a picture that is more consistent with most recent numbers of global C budgets suggested by Aufdenkampe et al. (2011). While the flux term of our budget may represent a low limit estimate, further research and more quantitative data are needed in order to improve our understanding of the interconnected link between river and wetlands and to better constrain the role of aquatic systems as a whole in both regional and global C budgets.

BGD
11, 16391–16445, 2014

5 Concluding remarks

Overall, results of this catchment scale study demonstrate that riverine GHGs, despite their interannual and seasonal variations, appeared to be mainly controlled by the connectivity with floodplains/wetlands, the presence of rapids/waterfalls and the existence of large man-made structures along the aquatic continuum. Although TA, $\delta^{13}C_{DIC}$ and DSi : Ca^{2+} values suggest the importance of both carbonate weathering as well as in-stream processes in controlling riverine DIC, the co-variation of pCO_2 with CH_4 suggest that dissolved gases in this river system originate largely from organic matter degradation. While comparable with other studied river systems in Africa, the range in GHG concentrations and fluxes in the Zambezi River Basin are below literature-based value for tropical rivers, streams and lakes/reservoirs. A C mass balance for the entire river suggest that GHG emission to the atmosphere represent less than 40 % of the total budget, with C export to the ocean (mostly as DIC) being the dominant component (59 %). However, the importance of GHG emissions in the overall budget is likely underestimated since our analyses do not take into account fluxes from the entire hydrological network (i.e. all tributaries), and since potentially large emissions that occur in the seasonally flooded wetlands and floodplains have not been estimated.

The Supplement related to this article is available online at doi:10.5194/bgd-11-16391-2014-supplement.

Acknowledgements. Funding for this work was provided by the European Research Council (ERC-StG240002, AFRIVAL – African river basins: catchment-scale carbon fluxes and transformations, http://ees.kuleuven.be/project/afrival/) and the Research Foundation Flanders (FWO-Vlaanderen, travel grants K2.011.12N and K2.266.13N to Cristian R. Teodoru). Alberto V. Borges is a senior research associate at the FRS-FNRS. We thank Zita Kelemen (KU Leuven) for technical and laboratory assistance, Marc-Vincent Commarieu (University of Liège) for the TA measurements, Kristin Coorevits ans Stijn Baeken (KU Leuven) for ICP-MS measurements, Peter Salaets (KU Leuven) for nutrient analyses, and Stephan Hoornaert and Sandro

Petrovic (University of Liège) who carried out part of the CH_4 measurements. We thank all generous and helpful people (Maurice Diamond, Sam Talbot, Tony Weber, Ann-Marie Butzelaar, Andrew Peter Dekker, and many others) for logistical support during sampling.

References

Abril, G., Martinez. J. M., Artigas, L. F., Moreira-Turcq. P., Benedetti, M. F., Vidal, L., Meziane, T., Kin, J. H., Bernardes, M. C., Savoye, N., Deborde, J., Souza, E. L., Albéric, P., Landim de Souza, M. F., and Roland, F.: Amazon River carbon dioxide outgassing fuelled by wetlands, Nature, 505, 395–398, doi:10.1038/nature12797, 2014a.

Abril, G., Bouillon, S., Darchambeau, F., Teodoru, C. R., Marwick, T. R., Tamooh, F., Omengo, F. O., Geeraert, N., Deirmendjian, L., Polsenaere, P., and Borges, A. V.: Technical Note: Large overestimation of $p\mathrm{CO_2}$ calculated from pH and alkalinity in acidic, organic-rich freshwaters, Biogeosciences Discuss., 11, 11701–11725, doi:10.5194/bgd-11-11701-2014, 2014b.

Amiotte-Suchet, P., Aubert, D., Probst, J. L., Gauthier-Lafaye, F., Probst, A., Andreux, F., and Viville, D.: δ^{13}C pattern of dissolved inorganic carbon in a small granitic catchment: the Strengbach case study (Vosges mountains, France), Chem. Geol., 159, 129– 145, 1999.

Ashton, P. J., Love, D., Mahachi, H., and Dirks, P. H. G. M.: An overview of the impact of mining and mineral processing operations on water resources and water quality in the Zambezi, Limpopo and Olifants Catchments in Southern Africa. Contract Report to the Mining, Minerals and Sustainable Development (SOUTHERN AFRICA). Project by CSIR-Environmentek, Pretoria, South Africaand Geology Department, University of Zimbabwe, Harare, Zimbabwe, Rep. ENV-P-C 2001–042, 336 pp., available at: http://pubs.iied.org/pdfs/G00599.pdf (last access: 15 September 2014), 2001.

Aufdenkampe, E. K., Mayorga, E., Raymond, P. A., Melack, J. M., Doney, S. C., Alin, S. R., Aalto, R. E., and Yoo, K.: Rivers key to coupling biogeochemical cycles between land, oceans and atmosphere, Front. Ecol. Environ. 9, 53–60, doi:10.1890/100014, 2011.

Bastviken, D., Tranvik, L. J., Downing, J. A., Crill, P. M., and Enrich-Prast, A.: Freshwater methane emissions offset the continental carbon sink, Science, 331, 6013, doi:10.1126/science.1196808, 2011.

Battin, T. J., Luyssaert, S., Kaplan, L. A., Aufdenkampe, A. K., Richter, A., and Tranvik, L. J.: The boundless carbon cycle, Nat. Geosci., 2, 598–600, doi:10.1038/ngeo618, 2009.
Beilfuss, R. and dos Santos, D.: Patterns of hydrological change in the Zambezi Delta, Mozambique. Working Paper #2: Program for the sustainable management of Cahora Bassa Dam and the Lower Zambezi Valley, USA, International Crane Foundation, Direcção Naçional de Aguas, Mozambique, 2001.
Bouillon, S., Abril, G., Borges, A. V., Dehairs, F., Govers, G., Hughes, H. J., Merckx, R., Meysman, F. J. R., Nyunja, J., Osburn, C., and Middelburg, J. J.: Distribution, origin and cycling of carbon in the Tana River (Kenya): a dry season basin-scale survey from headwaters to the delta, Biogeosciences, 6, 2475–2493, doi:10.5194/bg-6-2475-2009, 2009.
Bouillon, S., Yambélé, A., Spencer, R. G. M., Gillikin, D. P., Hernes, P. J., Six, J., Merckx, R., and Borges, A. V.: Organic matter sources, fluxes and greenhouse gas exchange in the Oubangui River (Congo River basin), Biogeosciences, 9, 2045–2062, doi:10.5194/bg-9-2045-2012, 2012.
Bouillon, S., Yambélé, A., Gillikin, D. P., Teodoru, C. R., Darchambeau, F., Lambert, T., and Borges, A. V.: Contrasting biogeochemical characteristics of the Oubangui River and tributaries (Congo River basin), Sci. Rep.,4, 5402, doi:10.1038/srep05402, 2014.
Briggs, D. A. and Mitchell, C. J.: Mineralogy and beneficiation of some industrial minerals from Zambia, Zamb, J. Appl. Earth Sci., 5, 18–27, 1991.
Butman, D. and Raymond, P. A.: Significant efflux of carbon dioxide from streams and rivers in the United States, Nat. Geosci., 4, 839–842, doi:10.1038/ngeo1294, 2011.
Cole, J. J. and Caraco, N. F.: Carbon in catchments: connecting terrestrial carbon losses with aquatic metabolism, Mar. Freshwater Res., 52, 101–110, 2001.
Cole, J. J., Prairie, Y. T., Caraco, N. F., McDowell, W. H., Tranvik, L. J., Striegl, R. G., Duarte, C. M., Kortelainen, P., Downing, J. A., Middelburg, J. J., and Melack, J.: Plumbing the global carbon cycle: integrating inland waters into the terrestrial carbon budget, Ecosystems, 10, 171–184, 2007.
Chenje, M.: State of the Environment Zambezi Basin 2000, SADC, IUCN, ZRA, and SARDC, Maseru, Lusaka and Harare, 334 pp., ISBN 978–1-77910-009-2, 2000.
Dauchez, S., Legendre, L., and Fortier, L.: Assessment of simultaneous uptake of nitrogenous nutrients (^{15}N) and inorganic carbon (^{13}C) by natural phytoplankton populations, Mar. Biol., 123, 651–666, 1995.

BGD
11, 16391–16445, 2014

Spatial variability and temporal dynamics of GHG concentrations and fluxes along the Zambezi River

C. R. Teodoru et al.

Doctor, D. H., Kendall, C., Sebestyen, S. D., Shanley, J. B., Ohte, N., and Boyer, E. W.: Carbon isotope fractionation of dissolved inorganic carbon (DIC) due to outgassing of carbon dioxide from a headwater stream, Hydrol. Process., 22, 2410–2423, 2008.

Driscoll, C. T., Fuller, R. D., Schecher, W. D.: The role of organic acids in the acidification of surface waters in the eastern US, Water Air Soil Poll., 43, 21–40, 1989.

Einola, E., Rantakari, M., Kankaala, P., Kortelainen, P., Ojala, A., Pajunen, H., Mäkelä, S., and Arvola, L.: Carbon pools and fluxes in a chain of five boreal lakes: a dry and wet year comparison, J. Geophys. Res., 116, G03009, doi:10.1029/2010JG001636, 2011.

Finlay, J. C.: Controls of streamwater dissolved inorganic carbon dynamics in a forested watershed, Biogeochemistry, 62, 231–252, doi:10.1023/A:1021183023963, 2003.

Finlay, J. C. and Kendall, C.: Stable isotope tracing of temporal and spatial variability in organic matter sources to freshwater ecosystems, in: Stable Isotopes in Ecology and Environmental Science, 2nd edn., edited by: Michener, R. and Lajtha, K., Blackwell Publishing, Oxford, UK, 2007.

Garrels, R. M. and Mackenzie, F. T.: Evolution of Sedimentary Rocks, W. W. Norton, New York, 397 pp., 1971.

Gillikin, D. P. and Bouillon, S.: Determination of δ^{18}O of water and δ^{13}C of dissolved inorganic carbon using a simple modification of an elemental analyzer – isotope ratio mass spectrometer (EA-IRMS): an evaluation, Rapid Commun. Mass Sp., 21, 1475–1478, 2007.

Guasch, H., Armengol, J., Martiì, E., and Sabater, S.: Diurnal variation in dissolved oxygen and carbon dioxide in two low-order streams, Water Res., 32, 1067–1074, doi:10.1016/S0043-1354(97)00330-8, 1998.

Hemold, H. F.: Acid neutralizing capacity, alkalinity, and acid-base status of natural waters containing organic acids, Environ. Sci. Technol., 24, 1486–1489, 1990.

Hunt, C. W., Salisbury, J. E., and Vandemark, D.: Contribution of non-carbonate anions to total alkalinity and overestimation of $p\mathrm{CO_2}$ in New England and New Brunswick rivers, Biogeosciences, 8, 3069–3076, doi:10.5194/bg-8-3069-2011, 2011.

IPCC: Working group I contribution to the fifth assessment report (AR5) of the intergovernmental panel on climate change, in: Climate Change 2013: The Physical Science Basis, Cambridge University Press, Cambridge, United Kingdom and New York, NY, USA, 1552 pp., 2013.

Kling, G. W, Kipphut, G. W., and Miller, M. C.: Arctic lakes and streams as gas conduits to the atmosphere: implications for tundra carbon budgets, Science, 251, 298–301, doi:10.1126/science.251.4991.298, 1991.

Kling, H., Stanzel, P., and Preishuber, M.: Impact modelling of water resources development and climate scenarios on Zambezi River discharge, J. Hydrol. Reg. Stud., 1, 17–43, 2014.

Koné, Y. J. M., Abril, G., Kouadio, K. N., Delille, B., and Borges, A. V.: Seasonal variability of carbon dioxide in the rivers and lagoons of Ivory Coast (West Africa), Estuar. Coast., 32, 246–260, 2009.

Koné, Y. J. M., Abril, G., Delille, B., and Borges, A. V.: Seasonal variability of methane in the rivers and lagoons of Ivory Coast (West Africa), Biogeochemistry, 100, 21–37, 2010.

Kunz, M. J., Anselmetti, F. S., Wuestm, A., Wehrli, B., Vollenweider, A., Thuring, S., and Senn, D. B.: Sediment accumulation and carbon, nitrogen, and phosphorus deposition in the large tropical reservoir Lake Kariba (Zambia/Zimbabwe), J. Geophys. Res., 116, G03003, doi:10.1029/2010JG001538, 2011a.

Kunz, M. J., Wuest, A., Wehrli, B., Landert, J., and Senn, D. B.: Impact of a large tropical reservoir on riverine transport of sediment, carbon and nutrients to downstream wetlands, Water Resour. Res., 47, W12531, doi:10.1029/2011WR010996, 2011b.

Lewis, E. and Wallace, D. W. R.: Program developed for CO_2 system calculations. ORNL/CDIAC-105, published by Carbon Dioxide Information Analysis Center, Oak Ridge National Laboratory, U.S. Department of Energy, Oak Ridge, Tennessee, 1998.

Ludwig, W., Probst, J.-L., and Kempe, S.: Predicting the oceanic input of organic carbon by continental erosion, Global Biogeochem. Cy., 10, 23–41, 1996.

Mann, P. J., Spencer, E. G. M., Dinga., B. J., Poulsen, J. R., Hernes, P. J., Fiske, G., Salter, M. E., Wang, Z. A., Hoering, K. A., Six, J., and Holmes, R. M.: The biogeochemistry of carbon across a gradient of streams and rivers within the Congo Basin, J. Geophys. Res.-Biogeo., 119, 687–702, 2014.

Marwick, T. R., Tamooh, F., Ogwoka, B., Teodoru, C., Borges, A. V., Darchambeau, F., and Bouillon, S.: Dynamic seasonal nitrogen cycling in response to anthropogenic N loading in a tropical catchment, Athi–Galana–Sabaki River, Kenya, Biogeosciences, 11, 443–460, doi:10.5194/bg-11-443-2014, 2014.

McCartney, M. P. and Houghton-Carr, H. A.: Modelling approach to assess inter-sectoral competition for water resources in the Kafue Flats, Zambia, J. Chart. Inst. Water E., 12, 101–106, doi:10.1111/j.1747-6593.1998.tb00157.x, 1998.

McCartney, M., Cai, X., and Smakhtin, V.: Evaluating the flow regulating functions of natural ecosystems in the Zambezi River Basin, IWMI Res. Rep. 148, International Water Management Institute (IWMI), Colombo, Sri Lanka, 59 pp., doi:10.5337/2013.206, 2013.

Mengis, M. R., Gächter, R., and Wehrli, B.: Sources and sinks of nitrous oxide (N_2O) in deep lakes, Biogeochemistry, 38, 281–301, 1997.

Meybeck, M.: Global chemical-weathering of surficial rocks estimated from river dissolved loads, Am. J. Sci., 287, 401–428, 1987.

Millero, F. J.: The thermodynamics of the carbonic acid system in seawater, Geochim. Cosmochim. Ac., 43, 1651–1661, 1979.

Moore, A. E., Cotterill, F. P. D., Main, M. P. L., and Williams, H. B.: The Zambezi River, in: Large Rivers: Geomorphology and Management, edited by: Gupta, A., John Wiley & Sons, Ltd, Chichester, UK, 311–333, 2007.

Mook, W. G., Koopmans, M., Carter, A. F., and Keeling, C. D.: Seasonal, latitudinal, and secular variations in the abundance and isotopic ratios of atmospheric carbon dioxide: 1. Results from land stations. J. Geophys. Res., 88, 10915–10933, 1983.

Mumba, M. and Thompson, J. R.: Hydrological and ecological impacts of dams on the Kafue Flats floodplain system, southern Zambia, Phys. Chem. Earth, 30, 442–447, 2005.

Parker, S. R., Poulson, S. R., Gammons, C. H., and Degrandpre, M. D.: Biogeochemical controls on diel cycling of stable isotopes of dissolved O_2 and dissolved inorganic carbon in the Big Hole River, Montana, Environ. Sci. Technol., 39, 7134–7140, 2005.

Rantakari, M. and Kortelainen, P.: Controls of total organic and inorganic carbon in randomly selected Boreal lakes in varied catchments, Biogeochemistry, 91, 151–162, 2008.

Raymond, P. A. and Cole, J. J.: Gas exchange in rivers and estuaries: choosing a gas transfer velocity, Estuaries, 24, 312–317, 2001.

Raymond, P. A., Hartmann, J., Lauerwald, R., Sobek, S., McDonald, C., Hoover, M., Butman, D., Striegl, R., Mayorga, E., Humborg, C., Kortelainen, P., Dürr, H., Meybeck, M., Ciais, P., and Guth, P.: Global carbon dioxide emissions from inland waters, Nature, 503, 355–359, doi:10.1038/nature12760, 2013.

Richardson, D. C., Newbold, J. D., Aufdenkampe, A. K., Taylor, P. G., and Kaplan, L. A.: Measuring heterotrophic respiration rates of suspended particulate organic carbon from stream ecosystems, Limnol. Oceanogr.-Meth., 11, 247–261, 2013.

BGD

11, 16391–16445, 2014

Spatial variability and temporal dynamics of GHG concentrations and fluxes along the Zambezi River

C. R. Teodoru et al.

Richey, J. E., Devol, A. H., Wofy, S. C., Victoria, R., and Riberio, M. N. G.: Biogenic gases and the oxidation and reduction of carbon in Amazon River and floodplain waters, Limnol. Oceanogr., 33, 551–561, 1988.

Richey, J. E., Melack, J. M., Aufdenkampe, A. K., Ballester, V. M., and Hess, L.: Outgassing from Amazonian rivers and wetlands as a large tropical source of atmospheric CO_2, Nature, 416, 617–620, 2002.

SADC, SARDC, GRID-Arendal, and ZAMCOM: Zambezi River Basin Atlas of the Changing Environment. Southern African Development Community (SADC), Southern African Research and Documentation Centre (SARDC), United Nations Environment Programme (UNEP)/GRID-Arendal, Zambezi Watercourse Commission (ZAMCOM), Gaborone, Harare and Arendal, 134 pp., 2012.

Sawakuchi, H. O., Bastviken, D., Sawakuchi, A. O., Krusche, A. V., Ballester, M. V. R., and Richey, J. E.: Methane emissions from Amazonian Rivers and their contribution to the global methane budget, Glob. Change Biol., 20, 2829–2840, doi:10.1111/gcb.12646, 2014.

Schlünz, B. and Schneider, R. R.: Transport of organic carbon to the oceans by rivers: re-estimating flux and burial rates, Int. J. Earth Sci., 88, 599–606, 2000.

Tamooh, F., Van den Meersche, K., Meysman, F., Marwick, T. R., Borges, A. V., Merckx, R., Dehairs, F., Schmidt, S., Nyunja, J., and Bouillon, S.: Distribution and origin of suspended matter and organic carbon pools in the Tana River Basin, Kenya, Biogeosciences, 9, 2905–2920, doi:10.5194/bg-9-2905-2012, 2012.

Tamooh, F., Borges, A. V., Meysman, F. J. R., Van Den Meersche, K., Dehairs, F., Merckx, R., and Bouillon, S.: Dynamics of dissolved inorganic carbon and aquatic metabolism in the Tana River basin, Kenya, Biogeosciences, 10, 6911–6928, doi:10.5194/bg-10-6911-2013, 2013.

Teodoru, C. R., del Giorgio, P., Prairie, Y. T., and Camire, M.: $p\mathrm{CO}_2$ dynamics in boreal streams of northern Quebec, Canada, Global Biogeochem. Cy., 23, GB2012, doi:10.1029/2008GB003404, 2009.

Teodoru, C. R., del Giorgio, P., and Prairie, Y. T.: Spatial heterogeneity of surface CO_2 fluxes in a newly created Eastmain-1 reservoir in northern Quebec, Canada, Ecosystems, 14, 28–46, doi:10.1007/s10021-010-9393-7, 2010.

Tranvik, L. J., Downing, J. A., Cotner, J. B., Loiselle, S. A., Striegl, R. G., Ballatore, T. J., Dillon, P., Finlay, K., Knoll, L. B., Kortelainen, P. L., Kutser, T., Larsen, S., Laurion, I., Leech, D. M., McCallister, L. S., McKnight, D. M., Melack, J. M., Porter, J. A., Prairie, Y. T., Renwick, W. H., Roland, F., Sherman, B. S., Schindler, D. W., Sobeck, S., Tremblay, A.,

BGD

11, 16391–16445, 2014

Spatial variability and temporal dynamics of GHG concentrations and fluxes along the Zambezi River

C. R. Teodoru et al.

Vanni, M. J., Verschoor, A. M., von Wachenfelds, E., and Weyhenmeyer, G. A.: Lakes and reservoirs as regulators of carbon cycling and climate, Limnol. Oceanogr., 54, 2298–2314, doi:10.4319/lo.2009.54.6_part_2.2298, 2009.

Vogel, J. C.: Variability of carbon isotope fractionation during photosynthesis, in: Stable Isotopes and Plant Carbon-water Relations, edited by: Saugier, B., Ehleringer, J. R., Hall, A. E., and Farquhar,G. D., Elsevier Inc, San Diego, California, USA, 29–46, 1993.

Waldron, S., Scott, E. M., and Soulsby, C.: Stable isotope analysis reveals lower-order river dissolved inorganic carbon pools are highly dynamic, Environ. Sci. Technol., 41, 6156–6162, doi:10.1021/es0706089, 2007.

Wang, Z. A., Bienvenu, D. J., Mann, P. J., Hoering, K. A., Poulsen, J. R., Spencer, R. G. M., and Holmes, R. M.: Inorganic carbon speciation and fluxes in the Congo River, Geophys. Res. Lett., 40, 511–516, doi:10.1002/grl.50160, 2013.

Weiss, F. R. and Price, B. A.: Nitrous oxide solubility in water and seawater, Mar. Chem., 8, 347–359, 1980.

Weiss, R. F.: Determinations of carbon dioxide and methane by dual catalyst flame ionization chromatography and nitrous oxide by electron capture chromatography, J. Chromatogr. Sci., 19, 611–616, 1981.

Wellington, J. H.: Southern Africa – a Geographic Study, vol. 1, Physical Geography, Cambridge University Press, Cambridge, 528 pp., 1955.

Whitfield, P. H., Aherne, J., and Watmough, S.: Predicting the partial pressure of carbon dioxide in boreal lakes, Can. Water Resour. J., 34, 415–426, 2009.

World Bank.: The Zambezi River Basin. A multi-sector investment opportunities analysis, vol. 3: State of the basin, published by the International Bank for Reconstruction and Development/The World Bank, 1818 H Street NW, Washington DC 20433, USA, 2010.

Worrall, F., Burt, T., and Adamson, J.: Fluxes of dissolved carbon dioxide and inorganic carbon from an upland peat catchment: implications for soil respiration, Biogeochemistry, 73, 515–539, doi:10.1007/s10533-004-1717-2, 2005.

Zurbrügg, R., Wamulume, J., Kamanga, R., Wehrli, B., and Senn, D. B.: River-floodplain exchange and its effects on the fluvial oxygen regime in a large tropical river system (Kafue Flats, Zambia), J. Geophys. Res., 117, G03008, doi:10.1029/2011JG001853, 2012.

Yamamoto, S., Alcauskas, J. B., and Crozier, T. E.: Solubility of methane in distilled water and seawater, J. Chem. Eng. Data, 21, 78–80, 1976.

Table 1. (a) Carbon emission estimates based on measured CO_2 and CH_4 fluxes (this work) and carbon removal by deposition in reservoirs based on available published data (Kunz et al., 2011a, b); (b) carbon export loads to the ocean calculated using average literature river discharge at the Zambezi Delta and POC, DOC and DIC concentrations (this work) measured at the river mouth (ZBZ.19 and ZBZ.20) during 2012 and 2013 wet season campaigns; and (c) carbon mass balance components including yield, emission, deposition and export. Data marked with [a] represent areal fluxes recalculated for the entire surface including reservoirs. Carbon deposition in the Kafue Gorge and Cahora Bassa reservoirs [b] were estimated assuming same deposition rates of the Itezhi Tezhi and the Kariba reservoirs. All loads are expressed in $kt\,C\,yr^{-1}$ ($1\,kt = 10^3$ metric tons).

(a) River/Reservoir	Area [km^2]	CO_2 flux [$mg\,C\,m^{-2}\,d^{-1}$]	CH_4 flux	CO_2	CH_4	Emission [$kt\,C\,yr^{-1}$]	Deposition
Kafue River without reservoirs	287	2962	20.0	310	2.1	312	–
Itezhi Tezhi Reservoir	364	737	25.8	98	3.4	101	16
Kafue Gorge Reservoir	13	737	25.8	3	0.1	4	1[b]
Kafue River with reservoirs	664	1698[a]	23.3[a]	411	5.6	417	17
Zambezi River without reservoirs	1879	4291	45.0	2943	30.8	2974	–
Kariba Reservoir	5364	−141	5.2	−276	10.1	−266	120
Cahora Bassa Reservoir	2670	−356	1.4	−347	1.4	−346	60[b]
Zambezi River with reservoirs	9913	641[a]	11.7[a]	2319	42.3	2362	180
Zambezi and Kafue Rivers with reservoirs	10576	707[a]	12.4[a]	2731	48.0	2779	196

(b) River	Q [$m^3\,s^{-1}$]	POC	DOC [$mg\,L^{-1}$]	DIC	POC	DOC [$kt\,C\,yr^{-1}$]	DIC
Zambezi River at Delta	3779	2.6	2.2	30.8	306	263	3672

(c)	Yield	Emission	Deposition [$kt\,C\,yr^{-1}$]	Export	Emission	Deposition [%]	Export
Carbon Balance at Zambezi Delta	7215	2779	196	4240	38	3	59

BGD

11, 16391–16445, 2014

Spatial variability and temporal dynamics of GHG concentrations and fluxes along the Zambezi River

C. R. Teodoru et al.

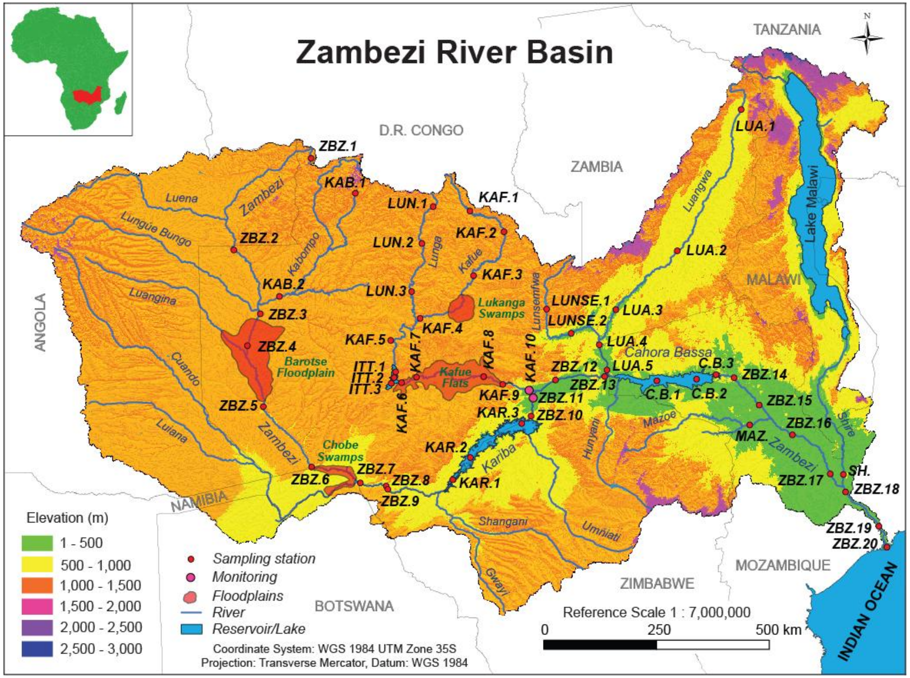

Figure 1. Map of the Zambezi River Basin illustrating the location within Africa, the shared area of the basin within the eight African nations, the elevation gradient, the main hydrological network and the distribution of sampling sites along the Zambezi mainstem and major tributaries.

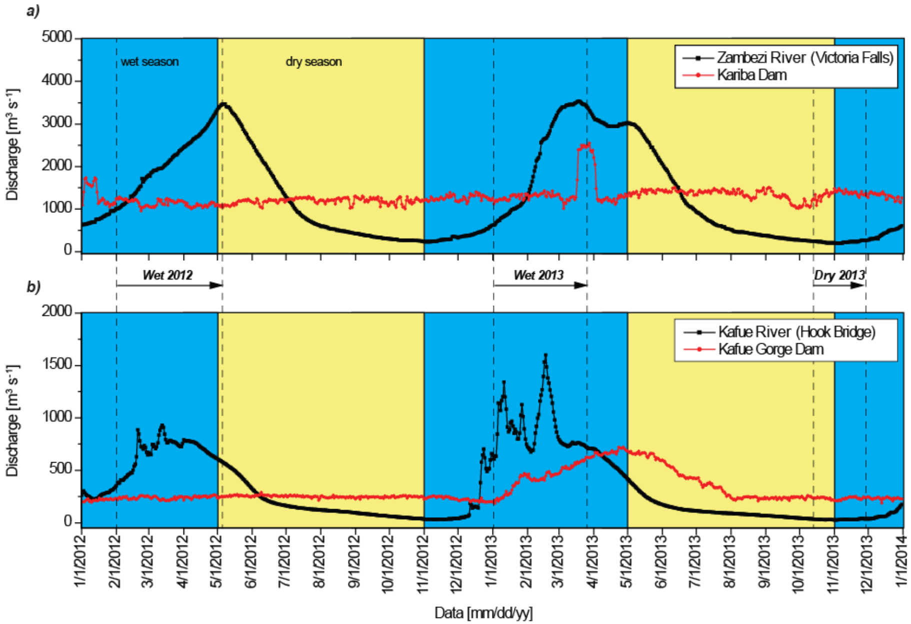

Figure 2. Water discharge for: **(a)** the Zambezi River at Victoria Falls power station and the disturbance of natural flow pattern by dam operation at Kariba Dam, and **(b)** for the Kafue River at the Hook Bridge (upstream of the Itezhi Tezhi Reservoir) and the regulated flow at the Kafue Gorge Dam between January 2012 and January 2014 (data from Zambia Electricity Supply Corporation Limited, ZESCO).

BGD

11, 16391–16445, 2014

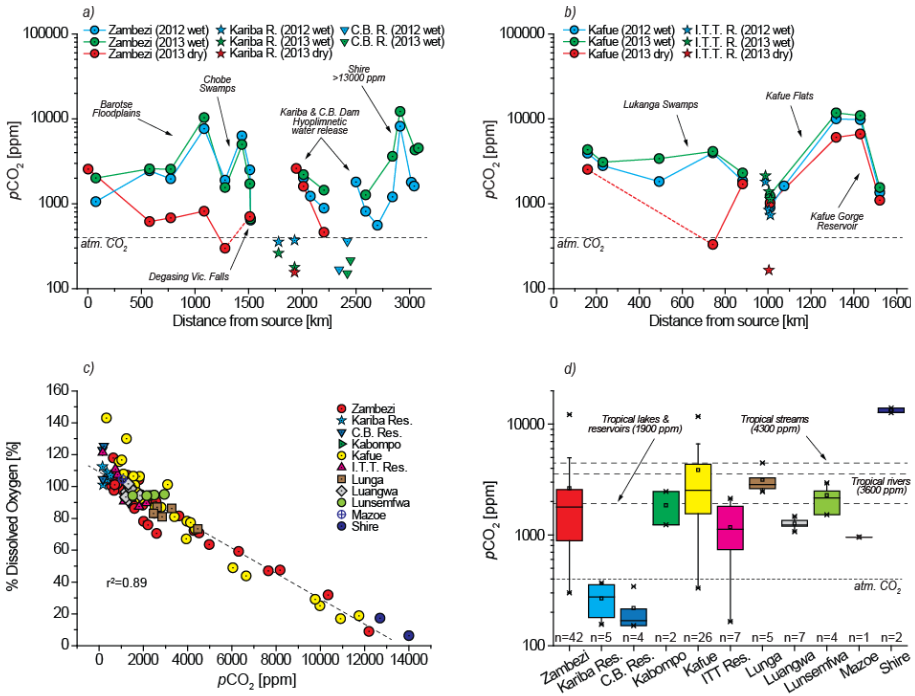

Figure 3. Spatial and temporal variability of pCO_2 (log scale) along: **(a)** the Zambezi River including the Kariba Reservoir (Kariba R.) and Cahora Bassa Reservoir (C.B. R), and **(b)** the Kafue River (log scale) including the Itezhi Tezhi Reservoir (I.T.T. R.); **(c)** the negative correlation between pCO_2 and dissolved oxygen (% DO) (linear scale); **(d)** global (all campaigns) range pCO_2 (log scale) for the Zambezi River, tributaries and reservoirs. Box-plot shows range, percentile, median, mean and outliers. Dot lines indicate global median pCO_2 values for tropical rivers, streams and lakes/reservoirs (Aufdenkampe et al., 2011).

BGD
11, 16391–16445, 2014

Title Page
Abstract | Introduction
Conclusions | References
Tables | Figures
◀| |▶
◀ ▶
Back | Close
Full Screen / Esc
Printer-friendly Version
Interactive Discussion

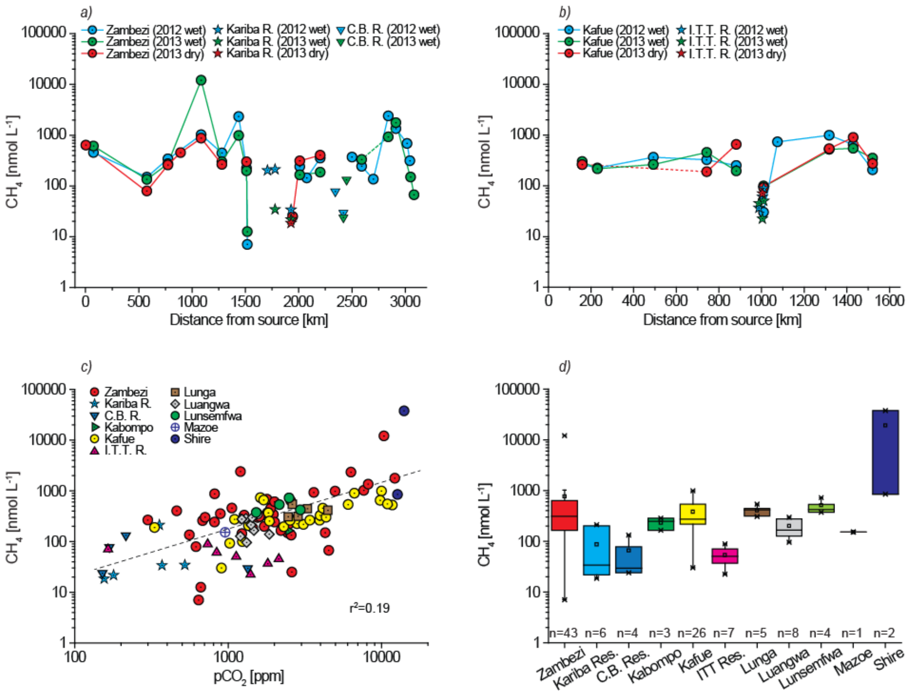

Figure 4. Spatial and temporal variability of CH_4 (log scale) along: **(a)** the Zambezi mainstem including the Kariba Reservoir (Kariba R.) and Cahora Bassa Reservoir (C.B. R), and **(b)** the Kafue River (log scale) including the Itezhi Tezhi Reservoir (I.T.T. R.); **(c)** the correlation between CH_4 and pCO_2 (log-log scale); **(d)** global (all campaigns) range CH_4 concentration (log scale) for the Zambezi River, tributaries and reservoirs. Box-plot shows range, percentile, median, mean and outliers.

BGD
11, 16391–16445, 2014

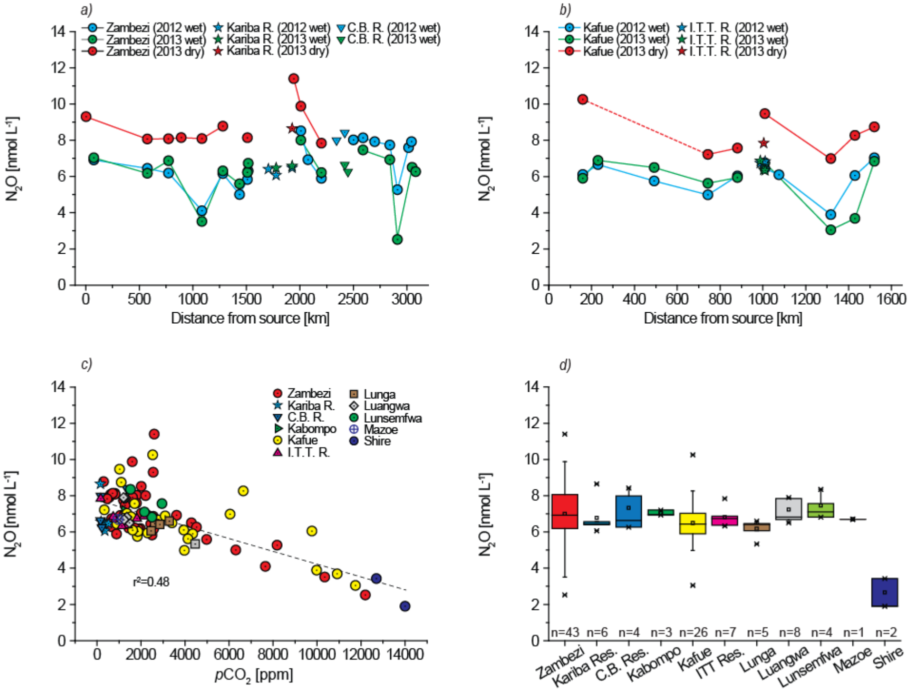

Figure 5. Spatial and temporal variability of N_2O along: **(a)** the Zambezi River including the Kariba Reservoir (Kariba R.) and Cahora Bassa Reservoir (C.B. R), and **(b)** the Kafue River including the Itezhi Tezhi Reservoir (I.T.T. R.); **(c)** the correlation between N_2O and pCO_2; **(d)** global (all campaigns) range N_2O concentration for the Zambezi River, tributaries and reservoirs. Box-plot shows range, percentile, median, mean and outliers.

BGD

11, 16391–16445, 2014

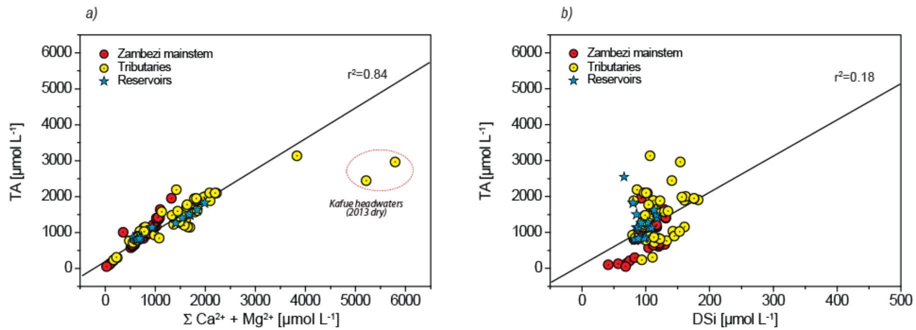

Figure 6. Relationships between the observed total alkalinity (TA) and: **(a)** the sum of Ca^{2+} and Mg^{2+}, and **(b)** dissolved silica (DSi).

BGD
11, 16391–16445, 2014

Spatial variability and temporal dynamics of GHG concentrations and fluxes along the Zambezi River

C. R. Teodoru et al.

Title Page
Abstract | Introduction
Conclusions | References
Tables | Figures
◀ | ▶
Back | Close
Full Screen / Esc
Printer-friendly Version
Interactive Discussion

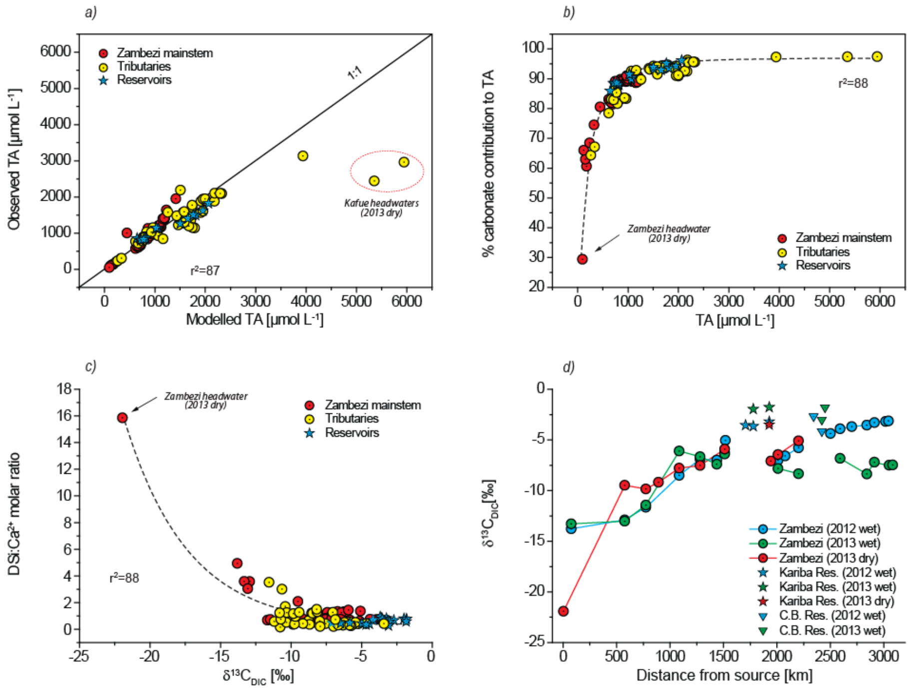

Figure 7. Relationships between: **(a)** modeled and observed total alkalinity (TA), **(b)** the estimated contribution of TA derived from carbonate weathering to observed TA (see text for details), and **(c)** isotopic signature of DIC ($\delta^{13}C_{DIC}$) to DSi : Ca^{2+} molar ratio; **(d)** the spatio-temporal variability of $\delta^{13}C_{DIC}$ along the Zambezi mainstem.

BGD
11, 16391–16445, 2014

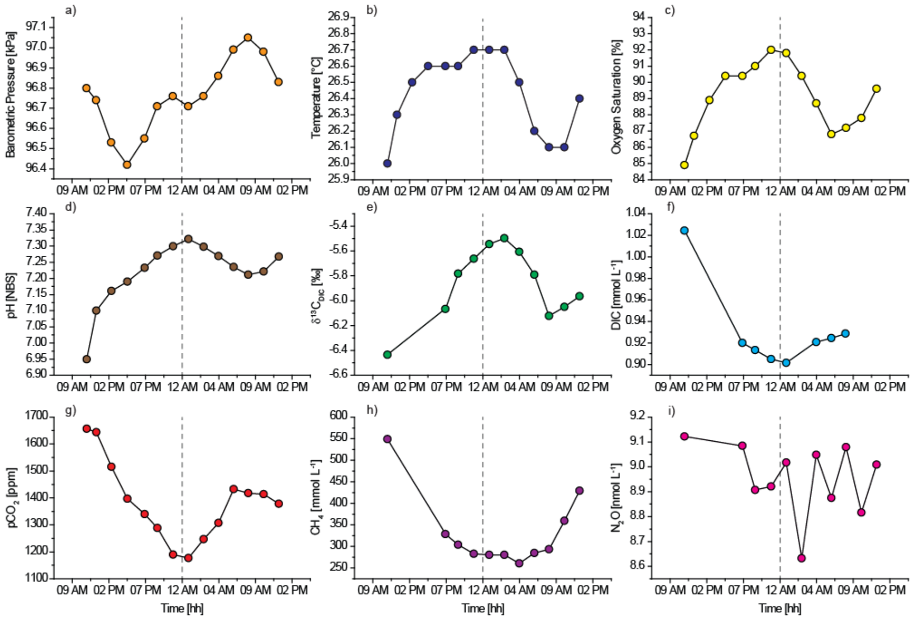

Figure 8. Dial variation of: **(a)** barometric pressure, **(b)** temperature, **(c)** dissolved oxygen saturation (%DO), **(d)** pH, **(e)** isotopic signature of dissolved inorganic carbon ($\delta^{13}C_{DIC}$), **(f)** dissolved inorganic carbon (DIC), **(g)** partial pressure carbon dioxide (pCO_2), **(h)** methane (CH_4), and **(i)** nitrous oxide (N_2O) measured at ZBZ.11 between 22 and 23 November 2013.

BGD
11, 16391–16445, 2014

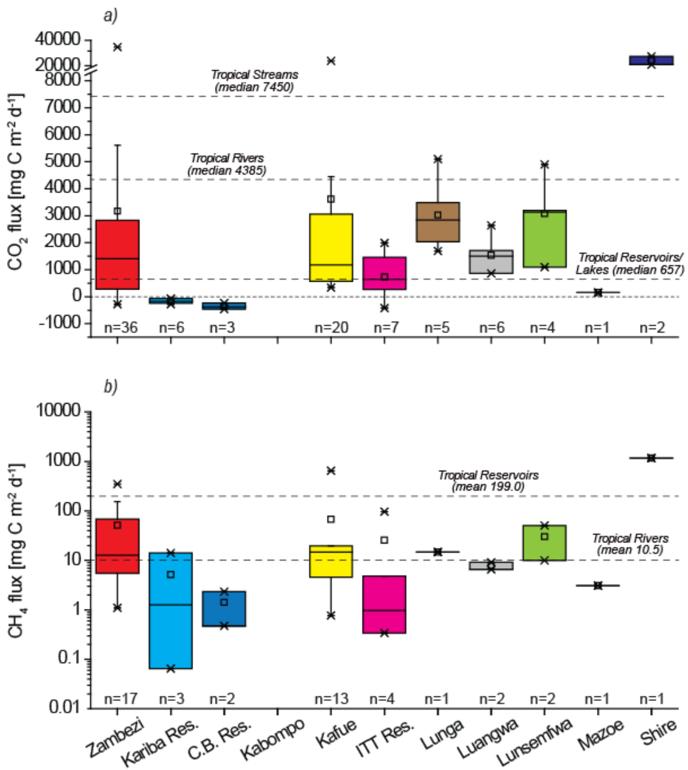

Figure 9. Measured range CO_2 (linear scale) **(a)**, and CH_4 fluxes (log scale) **(b)** for the Zambezi maintem, tributaries and reservoirs during the study period including both wet and dry seasons. Box-plot shows range, percentile, median, mean and outliers. Dot lines in **(a)** suggest global median CO_2 emission levels for tropical rivers, streams and lakes/reservoirs based on Aufdenkampe et al. (2011), while in **(b)** represent global mean CH_4 emission for tropical rivers and reservoirs based on Bastviken et al. (2011).

BGD
11, 16391–16445, 2014

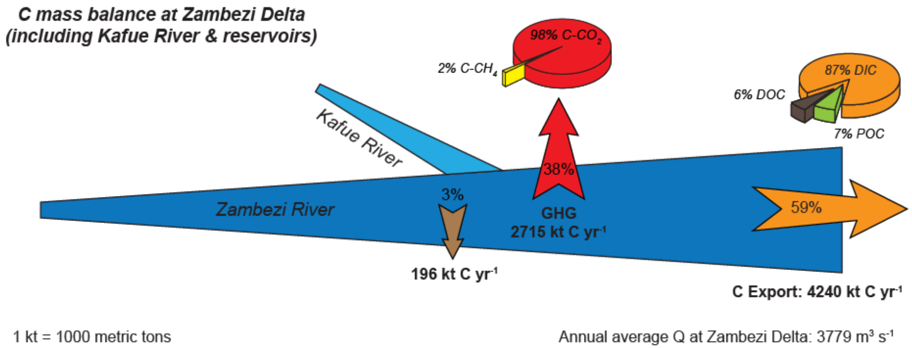

Figure 10. Carbon mass budget for the Zambezi River. GHG emission component was calculated for a total surface area of 10 576 km^2 out of which Zambezi mainstem represents 18 %, Kafue River accounts for 3 %, Itezhi Tezhi and Kafue Gorge reservoirs sum up to approximately 4 %, while Kariba and Cahora Bassa reservoirs represent 75 % (see Table 1).

BGD
11, 16391–16445, 2014

Spatial variability and temporal dynamics of GHG concentrations and fluxes along the Zambezi River

C. R. Teodoru et al.